



**HAL**  
open science

## Robust Evidence of $^{14}\text{C}$ , $^{13}\text{C}$ , and $^{15}\text{N}$ Analyses Indicating Fossil Fuel Sources for Total Carbon and Ammonium in Fine Aerosols in Seoul Megacity

Saehee Lim, Joori Hwang, Meehye Lee, Claudia Czimczik, Xiaomei Xu, Joel Savarino

► **To cite this version:**

Saehee Lim, Joori Hwang, Meehye Lee, Claudia Czimczik, Xiaomei Xu, et al.. Robust Evidence of  $^{14}\text{C}$ ,  $^{13}\text{C}$ , and  $^{15}\text{N}$  Analyses Indicating Fossil Fuel Sources for Total Carbon and Ammonium in Fine Aerosols in Seoul Megacity. *Environmental Science and Technology*, 2022, 56 (11), pp.6894-6904. 10.1021/acs.est.1c03903 . hal-04418357

**HAL Id: hal-04418357**

**<https://hal.science/hal-04418357>**

Submitted on 26 Jan 2024

**HAL** is a multi-disciplinary open access archive for the deposit and dissemination of scientific research documents, whether they are published or not. The documents may come from teaching and research institutions in France or abroad, or from public or private research centers.

L'archive ouverte pluridisciplinaire **HAL**, est destinée au dépôt et à la diffusion de documents scientifiques de niveau recherche, publiés ou non, émanant des établissements d'enseignement et de recherche français ou étrangers, des laboratoires publics ou privés.

# Robust Evidence of $^{14}\text{C}$ , $^{13}\text{C}$ , and $^{15}\text{N}$ Analyses Indicating Fossil Fuel Sources for Total Carbon and Ammonium in Fine Aerosols in Seoul Megacity

Saehee Lim, Joori Hwang, Meehye Lee,\* Claudia I. Czimczik, Xiaomei Xu, and Joel Savarino



Cite This: *Environ. Sci. Technol.* 2022, 56, 6894–6904



Read Online

ACCESS |



Metrics & More

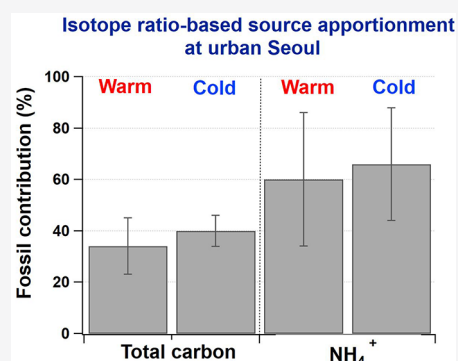


Article Recommendations



Supporting Information

**ABSTRACT:** Carbon- and nitrogen-containing aerosols are ubiquitous in urban atmospheres and play important roles in air quality and climate change. We determined the  $^{14}\text{C}$  fraction modern ( $f_M$ ) and  $\delta^{13}\text{C}$  of total carbon (TC) and  $\delta^{15}\text{N}$  of  $\text{NH}_4^+$  in the  $\text{PM}_{2.5}$  collected in Seoul megacity during April 2018 to December 2019. The seasonal mean  $\delta^{13}\text{C}$  values were similar to  $-25.1\text{‰} \pm 2.0\text{‰}$  in warm and  $-24.2\text{‰} \pm 0.82\text{‰}$  in cold seasons. Mean  $\delta^{15}\text{N}$  values were higher in warm ( $16.4\text{‰} \pm 2.8\text{‰}$ ) than in cold seasons ( $4.0\text{‰} \pm 6.1\text{‰}$ ), highlighting the temperature effects on atmospheric  $\text{NH}_3$  levels and phase-equilibrium isotopic exchange during the conversion of  $\text{NH}_3$  to  $\text{NH}_4^+$ . While  $37\% \pm 10\%$  of TC was apportioned to fossil-fuel sources on the basis of  $f_M$  values,  $\delta^{15}\text{N}$  indicated a higher contribution of emissions from vehicle exhausts and electricity generating units (power-plant  $\text{NH}_3$  slip) to  $\text{NH}_3$ :  $60\% \pm 26\%$  in warm season and  $66\% \pm 22\%$  in cold season, based on a Bayesian isotope-mixing model. The collective evidence of multiple isotope analysis reasonably supports the major contribution of fossil-fuel-combustion sources to  $\text{NH}_4^+$ , in conjunction with TC, and an increased contribution from vehicle emissions during the severe  $\text{PM}_{2.5}$  pollution episodes. These findings demonstrate the efficacy of a multiple-isotope approach in providing better insight into the major sources of  $\text{PM}_{2.5}$  in the urban atmosphere.



**KEYWORDS:**  $\text{PM}_{2.5}$ , ammonium, total carbon, stable isotopes, radiocarbon isotope, isotopic exchange equilibrium, source apportionment

## INTRODUCTION

Carbonaceous aerosol is ubiquitous in the atmosphere, contributing 20%–90% of the total concentration of fine aerosol mass and playing an important role with respect to air quality and climate.<sup>1,2</sup> The deterioration in air quality caused by secondary aerosol formation involving carbonaceous compounds may cause social and health issues. Carbonaceous aerosol can be divided into organic carbon (OC) and elemental carbon (EC). The OC is emitted directly or forms as secondary OC through gas-to-particle conversion during complex chemical and physical processes that are not fully understood.<sup>3</sup> The EC enters the atmosphere directly from incomplete combustion of biomass and fossil fuel, and strongly absorbs light, thereby affecting climate.<sup>4,5</sup>

Together with carbonaceous aerosol, secondary inorganic aerosol (SIA, including  $\text{NO}_3^-$ ,  $\text{SO}_4^{2-}$ , and  $\text{NH}_4^+$ ) is an important component of  $\text{PM}_{2.5}$  (particulate matter with a diameter  $\leq 2.5 \mu\text{m}$ ) haze pollution in East Asia.<sup>6–9</sup> It is generally understood that SIA is formed mainly when gaseous  $\text{NH}_3$  reacts with acidic gases such as  $\text{H}_2\text{SO}_4$  and  $\text{HNO}_3$ . Because of its critical role in the formation of SIA, the sources of  $\text{NH}_3$ , its gas-to-particle conversion processes, and its role in haze development are of considerable interest. Given the frequent occurrence of severe haze episodes characterized by high SIA levels, particular attention has been paid to  $\text{NH}_3$

emission sources that lead to the formation of SIA. While  $\text{NO}_3^-$  and  $\text{SO}_4^{2-}$  aerosols originate mainly from fossil-fuel combustion, the major sources of  $\text{NH}_3$  in urban areas are still debated. Although agricultural emissions are the largest sources of  $\text{NH}_3$  globally,<sup>10,11</sup> there is growing evidence that fossil fuel related and other sources may compete with agricultural sources in urban areas.<sup>6,12–14</sup>

Radiocarbon ( $^{14}\text{C}$ ) serves as a useful tool in distinguishing between fossil (e.g., vehicular emissions and coal combustion) and contemporary (nonfossil, e.g., biomass burning and biogenic emissions) sources of atmospheric particulate matter.<sup>15,16</sup> Fossil fuels are depleted in  $^{14}\text{C}$  due to radioactive decay over a long time compared with the  $^{14}\text{C}$  half-life (5730 years), while contemporary sources have similar  $^{14}\text{C}$  contents to atmospheric  $\text{CO}_2$ . The  $^{14}\text{C}/^{12}\text{C}$  ratio is usually reported as the “fraction modern ( $f_M$ )”, indicating the fractional contribution of modern sources to carbonaceous aerosols.<sup>17</sup>

**Special Issue:** Urban Air Pollution and Human Health

**Received:** June 14, 2021

**Revised:** March 2, 2022

**Accepted:** March 3, 2022

**Published:** April 8, 2022



Stable carbon and nitrogen isotopic ratios are also useful in attributing emission sources and tracing aerosol formation/transformation processes.<sup>6,18</sup> The attribution of atmospheric particulate matter to emission sources using stable carbon and nitrogen isotope compositions ( $\delta^{13}\text{C}$  and  $\delta^{15}\text{N}$ ) takes advantage of the relatively distinctive isotopic ratios of their source endmembers. For example, among reported  $\delta^{13}\text{C}$  values of fossil fuel endmembers, the  $\delta^{13}\text{C}$  values of carbonaceous particles emitted from gaseous fossil fuels ( $-40\%$  to  $-28\%$ <sup>19</sup>) are much lower than those from coal combustion ( $-23.4\% \pm 1.3\%$ <sup>19–22</sup>) and liquid fossil fuels ( $-25.5\% \pm 1.3\%$ <sup>19,20,23–29</sup>). The  $\delta^{15}\text{N}$  values of  $\text{NH}_3$  emitted from vehicular fossil-related sources ( $6.6\% \pm 2.1\%$ <sup>30</sup>) and power-plant  $\text{NH}_3$  slip ( $-12.95\% \pm 1.65\%$ <sup>31</sup>) are significantly higher than those from nonfossil sources including volatilized fertilizer ( $-46\% \pm 5\%$ <sup>31,32</sup>), livestock waste ( $-28\% \pm 11\%$ <sup>31–33</sup>), and urban waste ( $-37.8\% \pm 3.6\%$ <sup>32</sup>). Isotopic analysis has been applied in atmospheric chemistry studies, providing insight into atmospheric processes from emission to removal, with wide usage in studies of urban and background areas in East Asia.<sup>6,18,34–39</sup> Such studies have shown that fossil-fuel-related sources make a greater contribution to  $\text{NH}_3$  levels than that estimated from emission inventories particularly in urban areas (e.g., Chang et al.,<sup>32</sup> Pan et al.,<sup>18,40,41</sup> and Zhang et al.<sup>42</sup>). In ambient samples,  $\delta^{15}\text{N}$  of  $\text{NH}_4^+$  was systematically higher than  $\delta^{15}\text{N}$  values of  $\text{NH}_3$  due to isotope fractionation between gas- and particulate-phase, regardless of source types.<sup>43,44</sup> The isotope fractionation effect is affected by complex factors such as ambient temperature, ammonium partition ratio, and aerosol acidity, which makes it less straightforward to interpret the  $\delta^{15}\text{N}$  of  $\text{NH}_4^+$  in ambient samples.<sup>41,45</sup> Given that  $f_M$  distinguishes between fossil and nonfossil sources of carbonaceous aerosols, multiple carbon and nitrogen isotope ratios of aerosols are measured simultaneously help to understand atmospheric  $\delta^{15}\text{N}$  ( $\text{NH}_4^+$ ) variations and thus better constrain  $\text{NH}_3$  emissions. Consequently, combined isotopic ratios would be advantageous for identifying the sources of complex entities such as  $\text{PM}_{2.5}$  aerosols. Although there is a growing body of research on  $\delta^{15}\text{N}$  ( $\text{NH}_x$ ), measurements of seasonal variations in  $\delta^{15}\text{N}$  ( $\text{NH}_4^+$ ) are still scarce.<sup>35,40,42,44</sup> Here we present long-term multiple isotopic ratios in  $\text{PM}_{2.5}$  measured in Seoul, Korea, including  $\Delta^{14}\text{C}$ , defined as the radiocarbon composition, and  $\delta^{13}\text{C}$  values of total carbon ( $\text{TC} = \text{OC} + \text{EC}$ ) and  $\delta^{15}\text{N}$  values of  $\text{NH}_4^+$ . During the study period, record-breaking  $\text{PM}_{2.5}$  pollution episodes occurred in February–March 2019. Proportional contributions of seasonal emission sources to TC and  $\text{NH}_4^+$  in  $\text{PM}_{2.5}$  were estimated based on these isotopic ratios, elucidating transformation processes involving gas-to-particle conversion and photochemical reactions that lead to isotopic fractionation effects.

## MATERIALS AND METHODS

**Sampling and Chemical Analyses.** During April 2018 to December 2019, 92  $\text{PM}_{2.5}$  samples were collected at the Korea University campus in Seoul ( $37.59^\circ\text{N}$ ,  $127.02^\circ\text{E}$ ; Supporting Information (SI) Table S1). The  $\text{PM}_{2.5}$  was collected on quartz filters (Pallflex Products, Putnam, CT) for 1–3 days at a flow rate of  $68\text{ m}^3\text{ hr}^{-1}$  using a high-volume air sampler (3000 series, Ecotech, Australia). Filters were stored in a freezer pending chemical analysis. For  $\text{PM}_{2.5}$  chemical compositions, water-soluble ions ( $\text{Cl}^-$ ,  $\text{NO}_3^-$ ,  $\text{SO}_4^{2-}$ ,  $\text{Na}^+$ ,  $\text{NH}_4^+$ ,  $\text{K}^+$ ,  $\text{Ca}^{2+}$ , and  $\text{Mg}^{2+}$ ) and carbonaceous particulates (OC and EC) were determined by ion chromatography (IC; Eco-IC, Metrohm,

Switzerland) and by an OC-EC analyzer (Sunset Laboratory Inc., Portland, OR) with the thermo-optical transmittance method (NIOSH870), respectively. Water-soluble organic carbon (WSOC) was analyzed by a total organic carbon (TOC) analyzer (TOC-L, Shimadzu; at the Korea Basic Science Institute). TC and total nitrogen (TN) were analyzed by an elemental analyzer (EA, Fisons NA-1500NC, Thermo, Waltham, MA). All mass concentrations were corrected for laboratory and field blanks. Details of analytical methods can be found in elsewhere.<sup>6,39</sup> Hourly concentrations of  $\text{NH}_3$  were adopted from the previous work.<sup>46</sup>

**Isotopic Compositions:  $\Delta^{14}\text{C}$ ,  $\delta^{13}\text{C}$ , and  $\delta^{15}\text{N}$ .** Of the 92  $\text{PM}_{2.5}$  filter samples, 32 samples were analyzed for the three isotopic compositions including  $\Delta^{14}\text{C}$ ,  $\delta^{13}\text{C}$ , and  $\delta^{15}\text{N}$ , 31 samples for  $\Delta^{14}\text{C}$  and  $\delta^{13}\text{C}$ , and the remaining 29 samples for  $\delta^{13}\text{C}$ . The  $\Delta^{14}\text{C}$  and  $\delta^{13}\text{C}$  data covers the whole period, while  $\delta^{15}\text{N}$  data represent the nitrogen isotopic composition during May~August 2018 and December 2018~March 2019 (SI Table S1).

The  $^{14}\text{C}$  content of TC was determined for 63  $\text{PM}_{2.5}$  samples shipped frozen to the W. M. Keck Carbon Cycle AMS facility at UC Irvine. Multiple  $1.5\text{ cm}^2$  pieces of each filter were sealed with CuO (80 mg) under vacuum and combusted at  $900^\circ\text{C}$  for 3 h, yielding the  $\text{CO}_2$ . The  $\text{CO}_2$  of sample or blank was cryogenically purified and reduced to graphite using a sealed-tube zinc-reaction technique.<sup>47</sup> The graphite was then analyzed together with graphitization standards and blanks by accelerator mass spectrometry (AMS; NEC 0.5 MV 1.SSDH-1, National Electrostatics Corporation, Middleton, WI).<sup>48</sup> The  $^{14}\text{C}$  data are first calculated as  $\Delta^{14}\text{C}$  and reported as  $f_M$  values with  $^{13}\text{C}$  fractionation correction, using online AMS  $^{13}\text{C}/^{12}\text{C}$  calculations.<sup>49</sup> The uncertainty was  $2\%$ – $3\%$  (1 SD for long-term secondary standard analyses) for modern samples.

For all 92 samples, stable carbon isotopic ratios ( $\delta^{13}\text{C}$  values) were determined together with TC at UC Irvine, where TN concentrations were measured as well. The  $1.5\text{ cm}^2$  pieces (one or two) of each filter were analyzed with an EA system coupled to an isotope ratio mass spectrometry (IRMS; DeltaPlus XL, Thermo). Stable isotope ratios,  $\delta$  ( $\%$ ), is defined as  $(R_{\text{sample}}/R_{\text{standard}} - 1) \times 1000$ , where  $R$  is the ratio of  $^{13}\text{C}/^{12}\text{C}$  for stable carbon isotope or  $^{15}\text{N}/^{14}\text{N}$  for stable nitrogen isotope and  $R_{\text{sample}}$  ( $R_{\text{standard}}$ ) is the  $R$  of a sample (the international standard). We analyzed samples together with standards and field blanks and their  $\delta^{13}\text{C}$  values are reported relative to Vienna Pee Dee Belemnite (VPDB) with correction for filter and field blanks; uncertainty was  $0.1\%$ .

For the nitrogen isotopic composition of  $\text{NH}_4^+$  ( $n = 32$ ), the procedures of Kaiser et al.,<sup>50</sup> Morin et al.,<sup>51</sup> and Zhang et al.<sup>52</sup> were applied as follows. After solubilization of ammonium ions, sufficient volume (a few mL) of solution was taken to provide  $\sim 30\text{ nmol}$ . Following the procedure of Zhang et al.,<sup>52</sup> the ammonium was first converted to  $\text{NO}_2^-$  by  $\text{BrO}$  oxidation and then to  $\text{N}_2\text{O}$  by the azide method.<sup>53</sup> The  $\text{N}_2\text{O}$  was then flushed out with He and decomposed to  $\text{N}_2$  and  $\text{O}_2$  in a gold tube  $900^\circ\text{C}$ <sup>50</sup> using a fully automated system.<sup>51</sup> The  $\text{N}_2$  was used to determine the ammonium  $\delta^{15}\text{N}$  value by IRMS (MAT 253, Thermo). All liquid handling (sampling, dilution, reagent addition, and matrix matching) was performed automatically with a Gilson 215 liquid handler to minimize errors and variability between samples and standards. The  $\delta^{15}\text{N}$  values were based on calibrations involving International Atomic Energy Agency and U.S. Geological Survey ammonium sulfate standards IAEA-N-1, IAEA-N-2, USGS25, and USGS26.

Sample and standard analyses followed the “identical treatment principle”<sup>54</sup> with temperature, matrix, concentrations, and volumes being identical for samples and standards. Given the low ammonium blank (<2% on average) and low nitrite concentrations (<1% on an N basis), no blank/interference corrections were applied. The overall uncertainty was 0.3‰ (1 SD) for  $\delta^{15}\text{N}$ .<sup>51</sup>

**TC Source Apportionment.** The relative contributions of contemporary (nonfossil) sources ( $F_c$ ) and fossil fuel sources ( $F_{ff}$ ) can be estimated using  $f_M$  values of TC<sup>18</sup> as follows:

$$F_c(\text{TC}) = \{f_M(\text{TC}) - f_M(\text{ff})\} / \{f_M(c) - f_M(\text{ff})\} \quad (1)$$

$$F_{ff}(\text{TC}) = \{f_M(\text{TC}) - f_M(c)\} / \{f_M(\text{ff}) - f_M(c)\} \quad (2)$$

where  $f_M(c)$  and  $f_M(\text{ff})$  indicate the  $f_M$  values of contemporary sources and fossil-fuel sources, respectively. A mean value of  $f_M(c)$  was adopted for  $^{14}\text{CO}_2$  ( $1.0112 \pm 0.0026$ ;  $n = 38$ ), as measured at Point Barrow, Alaska, during January–May, 2018 (X. Xu, Pers. comm., 2019). The  $f_M(\text{ff})$  value was approximated as being zero.

**Simulations.** Bayesian stable isotope mixing model<sup>55</sup> implemented as SIMMR (full name: Stable Isotope Mixing Model in R) package in R software (<https://cran.r-project.org/web/packages/simmr/index.html>) was used for source apportionment of  $\text{NH}_4^+$  based on  $\delta^{15}\text{N}$  ( $\text{NH}_4^+$ ). As input data,  $\delta^{15}\text{N}$  ( $\text{NH}_3$ ) was estimated and previously reported  $\delta^{15}\text{N}$  values of major  $\text{NH}_3$  source endmembers were adopted (SI Table S2): 6.6‰  $\pm$  2.1‰ for vehicular fossil-related sources,<sup>30</sup> -12.95‰  $\pm$  1.65‰ for  $\text{NH}_3$  slip from power-plant equipped with selective catalytic reduction (SCR),<sup>31</sup> -46‰  $\pm$  5‰ for volatilized fertilizer,<sup>31,32</sup> -28‰  $\pm$  11‰ for livestock waste,<sup>31–33</sup> and -37.8‰  $\pm$  3.6‰ for urban waste.<sup>32</sup> Further information on the model can be found in Parnell et al.<sup>56</sup>

Two-day Backward trajectories of air masses were traced at 500 m above ground level (a.g.l.) every 6 h from the sampling site, using the U.S. National Oceanic and Atmospheric Administration (NOAA) HYSPLIT (Hybrid Single-Particle Lagrangian Integrated Trajectory) model with meteorological input data from the global data assimilation system based on a regular  $1^\circ \times 1^\circ$  longitude–latitude grid (<https://ready.arl.noaa.gov/HYSPLIT.php>).<sup>57</sup> Given the probability that an emission source is located at a certain latitude and longitude ( $i$  and  $j$ , respectively), the potential source contribution function (PSCF) was determined as the ratio of the number of trajectory end points associated with isotopic ratios above a threshold (here, the 95th percentile) to the total number of end points in the  $i, j$  grid cell. The PSCF analysis is available using the OPENAIR package in R (<https://cran.r-project.org/web/packages/openair/index.html>).<sup>58</sup>

## RESULTS AND DISCUSSION

**Seasonal Variations in  $\text{PM}_{2.5}$ .**  $\text{PM}_{2.5}$  concentrations varied over a wide range of 4.5–139.0  $\mu\text{g m}^{-3}$  during the experiment period. Given the distinct seasonality associated with synoptic weather patterns in East Asia,<sup>59</sup> measurements were divided into two seasonal groups, namely the “warm” season from April to September and the “cold” season from October to March (SI Figure S1).

The mean ( $\pm 1$  SD)  $\text{PM}_{2.5}$  concentrations were  $46.5 \pm 28.8 \mu\text{g m}^{-3}$  in the cold season and  $23.3 \pm 11.5 \mu\text{g m}^{-3}$  in the warm season. In general, the mass concentration of major  $\text{PM}_{2.5}$  constituents was higher in the cold season than in the warm season, while the seasonal variations in EC, WSOC, and  $\text{SO}_4^{2-}$

were less evident (Table 1).  $\text{PM}_1$  measured in Seoul also showed similar seasonal characteristics between SIA and

**Table 1. Seasonal  $\text{PM}_{2.5}$  Chemical and Isotopic Compositions in Seoul during April 2018 to December 2019 (Mean  $\pm 1$  SD)**

composition	warm season (April~September)	cold season (October~March)
$f_M(\text{TC})$	$0.6531 \pm 0.1141$	$0.6065 \pm 0.0651$
$\delta^{13}\text{C}$ (TC) <sup>a</sup>	$-25.1 \pm 2.0$	$-24.2 \pm 0.8$
$F_c(\%)$ ; $F_{ff}(\%)$	$66 \pm 11$ ; $34 \pm 11$	$60 \pm 6$ ; $40 \pm 6$
$\delta^{15}\text{N}$ ( $\text{NH}_4^+$ ) <sup>a,b</sup>	$16.4 \pm 2.8$	$4.0 \pm 6.1$
$\text{PM}_{2.5}$ ( $\mu\text{g m}^{-3}$ )	$23.3 \pm 11.5$	$46.5 \pm 28.8$
TC	$6.9 \pm 4.4$	$13.0 \pm 4.5$
OC	$4.0 \pm 2.1$	$7.3 \pm 2.0$
EC	$0.6 \pm 1.5$	$0.6 \pm 0.2$
OC/EC	$12.9 \pm 4.7$	$13.6 \pm 3.8$
WSOC	$2.1 \pm 1.7$	$2.5 \pm 1.1$
TN	$3.4 \pm 3.1$	$9.3 \pm 6.3$
$\text{NH}_4^+$	$2.6 \pm 2.1$	$7.1 \pm 6.3$
$\text{NO}_3^-$	$3.6 \pm 5.0$	$19.6 \pm 17.4$
$\text{SO}_4^{2-}$	$5.5 \pm 3.6$	$6.9 \pm 6.2$

<sup>a</sup>Weighted-means. <sup>b</sup>Warm and cold seasons include samples obtained during May~August and December~March, respectively.

nonrefractory concentrations, with noticeably higher  $\text{NO}_3^-$  and  $\text{NH}_4^+$  concentrations in the cold season and comparable  $\text{SO}_4^{2-}$  concentrations throughout the year.<sup>60</sup> Consequently, the mass contribution of nitrogen species to  $\text{PM}_{2.5}$  was substantially high in the cold season, whereas the contributions of carbonaceous species and  $\text{SO}_4^{2-}$  were relatively more important in the warm season when  $\text{PM}_{2.5}$  was low. The drastic increase in  $\text{NO}_3^-$  relative to  $\text{SO}_4^{2-}$  concentrations was also observed in Beijing during winter, when  $\text{PM}_{2.5}$  concentrations were highly elevated.<sup>7</sup>

The mean concentrations of TC and TN and TC/TN ratio were  $13.0 \pm 4.5 \mu\text{g m}^{-3}$ ,  $9.3 \pm 6.3 \mu\text{g m}^{-3}$ , and  $1.2 \pm 1.0$  in the cold season and  $6.9 \pm 4.4 \mu\text{g m}^{-3}$ ,  $3.4 \pm 3.1 \mu\text{g m}^{-3}$ , and  $2.7 \pm 2.5$  in the warm season, respectively (Table 1). The inorganic nitrogen mass ( $\text{NH}_4^+ + \text{NO}_3^-$ ) dominated TN in the cold season, exceeding TN concentration due to different analytical methods. In the warm season, the inorganic nitrogen mass accounted for 75% of TN, with 25% being attributed to organic nitrogen. The pronounced seasonality of  $\text{PM}_{2.5}$  levels and its composition have been described elsewhere (Lim et al., in press).<sup>61</sup>

### Emission Sources and Atmospheric Processing of TC.

In Seoul, the average contribution of contemporary ( $F_c$ ) and fossil fuels ( $F_{ff}$ ) sources to TC in  $\text{PM}_{2.5}$  was  $63\% \pm 10\%$  and  $37\% \pm 10\%$ , respectively (Table 1). While  $F_c$  was greater than  $F_{ff}$ ,  $F_{ff}$  was larger in the cold season ( $40\% \pm 6\%$ ) than in the warm season ( $34\% \pm 11\%$ ).

The average  $F_{ff}$  was comparable with those observed at urban sites globally (20%–60%; Heal et al.<sup>16</sup> and references therein) but lower than those of highly polluted megacities in China such as Beijing during 2013–2014 (40%–70% depending on season)<sup>62</sup> and spring 2016 ( $52\% \pm 7\%$ )<sup>6</sup> and Guangzhou during 2012 (42%).<sup>63</sup> In general, contemporary sources were predominant in rural areas and during warm periods. For example,  $F_c$  was  $76\% \pm 7\%$  at Taehwa Research Forest (TRF), a peri-urban forest site ~45 km south of Seoul, in summer and fall<sup>39</sup> and  $81\% \pm 10\%$  at an island site in

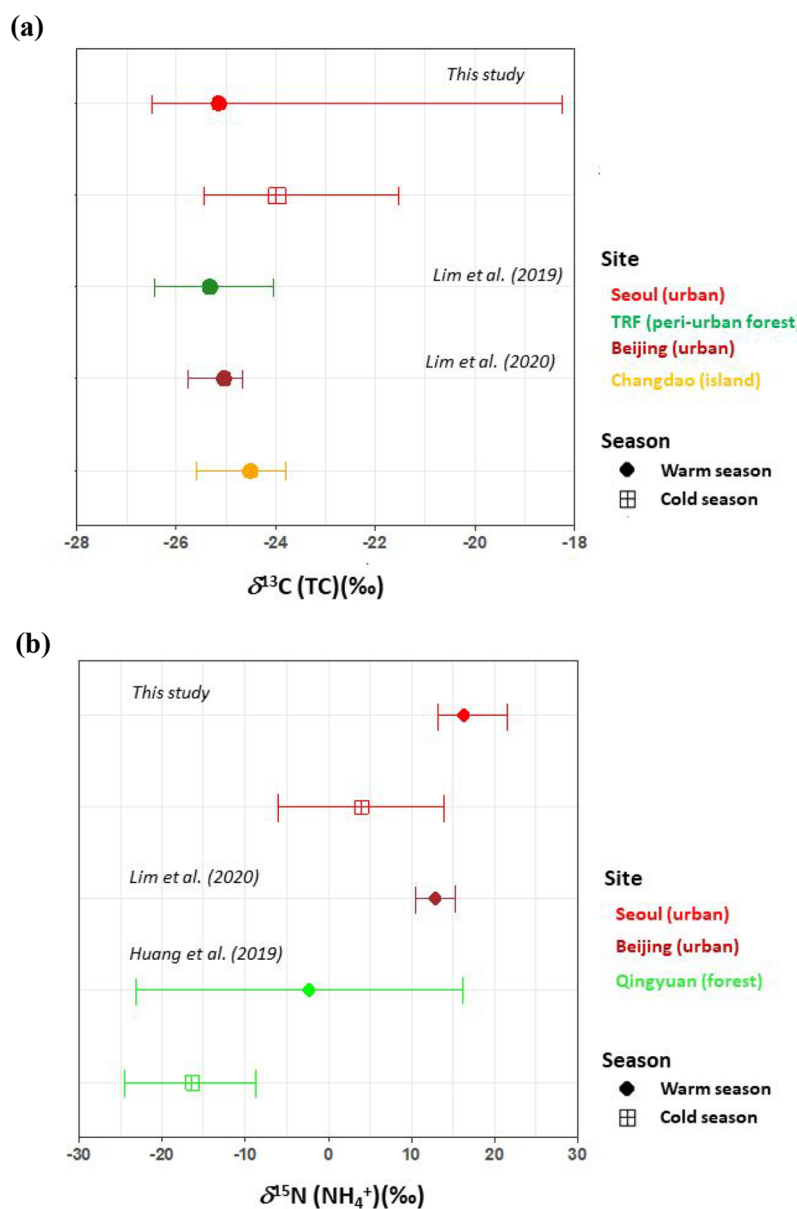


**Figure 1.** Ranges of  $\delta^{13}\text{C}$  (TC) (a) and  $\delta^{15}\text{N}$  ( $\text{NH}_4^+$ ) (b) of  $\text{PM}_{2.5}$  in Northeast Asia. Colors indicate different sites: Seoul (this study) in red; Taehwa Research Forest (TRF, summer and fall, 2014)<sup>39</sup> in green; Beijing (BJ, late spring, 2016)<sup>6</sup> in brown, Changdao (CD, late spring, 2016)<sup>6</sup> in orange, and Qingyuan Forest (QF, summer and winter, 2014–2016)<sup>35</sup> in pale green. Marker shapes indicate different seasons: warm season and cold season in circle and square, respectively. Points denote mean values (concentration-weighted means for Seoul) and error bars indicate minimum and maximum values.

China.<sup>64</sup> However, it is noteworthy that considering the high TC loadings in the cold season, fossil fuels are as important as contemporary sources for  $\text{PM}_{2.5}$  carbonaceous particles.

In addition to  $f_M$ ,  $\delta^{13}\text{C}$  provides further information about sources of carbonaceous particles using the available endmember values of  $\delta^{13}\text{C}$  (SI Table S3):  $-40\text{‰}$  to  $-28\text{‰}$  for carbonaceous particles from gaseous fossil fuels;<sup>19</sup>  $-33\text{‰}$  to  $-29\text{‰}$  for secondary organic aerosol (SOA) generated in laboratories;<sup>65,66</sup>  $-26.7\text{‰} \pm 1.8\text{‰}$  for C3 plants (wood);<sup>20,23,27,29,67–69</sup>  $-25.5\text{‰} \pm 1.3\text{‰}$  for liquid fossil fuels;<sup>19–22</sup> and  $-23.4\text{‰} \pm 1.3\text{‰}$  for coal combustion.<sup>19,20,23–29</sup> The highest  $\delta^{13}\text{C}$  were found in C4 plants ( $-12.8\text{‰} \pm 0.6\text{‰}$ <sup>69</sup>) and marine carbonaceous aerosols ( $\delta^{13}\text{C} = -22\text{‰}$  to  $-18\text{‰}$ <sup>70</sup>).

The  $\delta^{13}\text{C}$  values were distributed over a narrow range but slightly enriched in the cold season, with the weighted-mean  $\delta^{13}\text{C}$  (TC) of  $-25.1\text{‰} \pm 2.0\text{‰}$  and  $-24.2\text{‰} \pm 0.82\text{‰}$  for the warm and the cold seasons, respectively (Figure 1). When the entire range of  $\text{PM}_{2.5}$  concentration was divided into seven intervals from  $0\text{--}20 \mu\text{g m}^{-3}$  to  $120\text{--}140 \mu\text{g m}^{-3}$ ,  $f_M$  and  $\delta^{13}\text{C}$  were moderately correlated with  $\text{PM}_{2.5}$  concentrations, excepting the highest  $\text{PM}_{2.5}$  bins (above  $80 \mu\text{g m}^{-3}$ ) (Figure 2). This type of characteristic seasonality in isotopic ratios depending on  $\text{PM}_{2.5}$  concentrations is primarily driven by synoptic circulation, demonstrating that emission sources and formation processes of carbonaceous aerosol are significantly affected by meteorological conditions.

In the warm season, the  $\delta^{13}\text{C}$  values were similar to those observed at TRF<sup>39</sup> and at Beijing and Changdao in China<sup>6</sup>

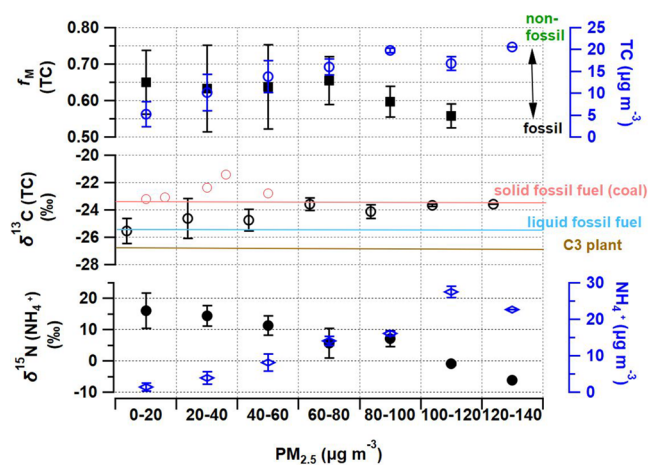


**Figure 2.** Source signatures of  $f_M$  (TC),  $\delta^{13}\text{C}$  (TC), and  $\delta^{15}\text{N}$  ( $\text{NH}_4^+$ ) as a function of  $\text{PM}_{2.5}$  mass concentration. In the center panel, pink open circles indicate upper bounds of  $\delta^{13}\text{C}$  (TC) data set.

(Figure 1a). The most depleted  $^{13}\text{C}$  ( $\delta^{13}\text{C}$  below  $-26\%$ ) was observed in marine air masses transported from the east or south of the Korean Peninsula with low  $\text{PM}_{2.5}$  concentrations ( $17.1 \pm 7.5 \mu\text{g m}^{-3}$ ), implying emissions from biomass combustion/biogenic emissions in remote regions and subsequent SOA formation during transport. In addition, the highest  $\delta^{13}\text{C}$  ( $-18.1\%$ ) possibly resulted from the  $\delta^{13}\text{C}$  values for soil organic matter, typically between  $-20\%$  and  $-15\%$ .<sup>71</sup> Excluding this extreme outlier, the mean  $\delta^{13}\text{C}$  of the warm season fell within the range of biomass (C3 plants) combustion to liquid fossil-fuels. As evidence supporting the contribution of biomass combustion, the TC/TN and WSOC/OC ratios were higher in the warm season ( $2.7 \pm 2.5$  and  $0.55 \pm 0.38$ , respectively) than in the cold season ( $1.2 \pm 1.0$  and  $0.36 \pm 0.19$ , respectively).

During the cold season,  $\delta^{13}\text{C}$  values shifted slightly toward the endmembers of coal combustion and were in the range between liquid fossil-fuel and coal combustion. Actually, the mean  $\delta^{13}\text{C}$  ( $-24.2\% \pm 0.8\%$ ) is in excellent agreement with what was observed in Changdao, China ( $-24.5\% \pm 0.44\%$ ; Figure 1a), which is an area influenced by coal combustion in highly populated areas.<sup>6</sup> A greater contribution of coal combustion is also in accordance with the  $\text{PM}_{2.5}$  chemical characteristics, showing lower WSOC/OC and volatile OC fraction of  $(\text{OC1} + \text{OC2})/\text{OC}$  compared to the warm season (Table 1). In Figure 2, the highest  $\delta^{13}\text{C}$  values above  $-23\%$  (i.e., above 95th percentile of  $\delta^{13}\text{C}$  observations; red circles in middle panel) are commensurate with endmembers of coal combustion. These samples are characterized by lower  $\text{NO}_3^-/\text{SO}_4^{2-}$  molar ratios ( $2.84 \pm 0.71$ ), higher TC/TN ratios ( $1.60 \pm 0.35$ ), similar  $f_M$  values, but much lower  $\text{PM}_{2.5}$  concentrations ( $24.5 \pm 15.5 \mu\text{g m}^{-3}$ ) than the seasonal mean (Table 1). During these periods, air masses passed over the northeast China such as Liaoning Province (SI Figure S2).

The record-breaking  $\text{PM}_{2.5}$  episode during 28 February to 6 March 2019 provided a unique opportunity to investigate emission sources and atmospheric processes under dynamic variations in  $\text{PM}_{2.5}$  concentrations. During the study period,  $\text{PM}_{2.5}$  concentrations greater than  $80 \mu\text{g m}^{-3}$  were encountered exclusively during this episode. In Figure 2 and SI Figure S3, it is evident that  $\delta^{13}\text{C}$  increased from  $-25.5\%$  to  $-23.6\%$  as the  $\text{PM}_{2.5}$  concentration increased from  $0\text{--}20 \mu\text{g m}^{-3}$  to  $60\text{--}80 \mu\text{g m}^{-3}$ , and above that ( $80\text{--}140 \mu\text{g m}^{-3}$ ) it remained high with a decrease in  $f_M$ . In this extreme episode,  $\text{NO}_3^-$  was dominated (up to  $69 \mu\text{g m}^{-3}$ ) and  $\text{SO}_4^{2-}$  remained relatively low (up to  $28 \mu\text{g m}^{-3}$ ), while TN and TC concentrations increased with  $\text{PM}_{2.5}$  concentrations. Air masses originated from heavily populated areas in the North China Plain (NCP) were slowly transported to Seoul metropolitan areas. The combined signatures of carbon isotopes and chemical composition imply a greater contribution of fossil fuel sources, further highlighting the key role of vehicle emissions in  $\text{PM}_{2.5}$  mass increase during the severe  $\text{PM}_{2.5}$  pollution episode. As discussed above, the seasonal characteristics of both  $f_M$  and  $\delta^{13}\text{C}$  indicate that the contribution of liquid fossil fuels to  $\text{PM}_{2.5}$  carbonaceous aerosols is significant year-round in Seoul.

It is noteworthy that four samples yielded  $f_M$  values exceeding  $>1$ , which are generally considered contaminated. Interestingly, three of them were obtained from a single winter episode, during which the air was highly stagnant. Their  $\text{PM}_{2.5}$  concentrations varied over a wide range (21, 97, and  $139 \mu\text{g m}^{-3}$ ), but  $\delta^{13}\text{C}$  values remained around the cold-season mean, suggesting unknown but fossil-fuel related  $^{14}\text{C}$  contamination sources in urban areas.

These findings demonstrate the efficacy of dual isotopic analysis including  $\delta^{13}\text{C}$  and  $f_M$  in source apportionment of carbonaceous aerosols. In addition, the stable carbon isotopic ratio is known to be affected by atmospheric photochemical processes.<sup>37,72</sup> For example, laboratory-formed secondary organic compounds showed a significant depletion in  $^{13}\text{C}$  relative to those of its precursors,<sup>66,73</sup> while particulate  $\delta^{13}\text{C}$  became considerably higher as being aged in outflow regions of East Asia.<sup>37,72</sup> These changes in  $\delta^{13}\text{C}$  largely resulted from the kinetic isotope effect (KIE) during atmospheric chemical reactions. In the present study,  $^{13}\text{C}$  was most depleted during the summer, and the minimum  $\delta^{13}\text{C}$  of about  $-26\%$  was found to be associated with a high  $f_M$  greater than 0.6 and a large contribution of volatile OC components ( $(\text{OC1} + \text{OC2})/\text{OC} \approx 0.4$ ). Therefore, the  $^{13}\text{C}$ -depleted carbonaceous particles were likely to be produced from gaseous precursors via photochemical reactions. The secondary formation fingerprint of carbonaceous aerosol was evident in summer when  $\text{PM}_{2.5}$  concentrations were low (Figure 2). Given the distinct seasonal features of  $\delta^{13}\text{C}$  in relation to  $\text{PM}_{2.5}$  mass, the measured  $\delta^{13}\text{C}$  values primarily reflect the emission sources of carbonaceous aerosol.

**Isotopic Fractionation During  $\text{NH}_3\text{--NH}_4^+$  Conversion.** In this study, the  $\text{NH}_4^+$  concentrations increased almost linearly with  $\text{PM}_{2.5}$  concentrations ( $R = 0.95$ ), demonstrating a pronounced role of SIA in  $\text{PM}_{2.5}$  mass increase. There were strong positive correlations between SIA species ( $R > 0.9$ ) as well. It is, therefore, crucial to understand the transformation of gas-phase  $\text{NH}_3(\text{g})$  to particulate  $\text{NH}_4^+(\text{p})$  in which acidic gases are neutralized and converted to the particle phase. For  $\delta^{15}\text{N}$  ( $\text{NH}_4^+$ ), the warm and cold seasons refer to June~August and December~mid-March, respectively.

Over the experiment period of  $\delta^{15}\text{N}$  ( $\text{NH}_4^+$ ), the  $\text{NH}_4^+$  concentration varied from  $0.1 \mu\text{g m}^{-3}$  to  $28.6 \mu\text{g m}^{-3}$  with a noticeably higher cold-season mean ( $11.7 \pm 8.4 \mu\text{g m}^{-3}$ ) than a warm-season mean ( $1.8 \pm 0.8 \mu\text{g m}^{-3}$ ) (Table 2), which is the same seasonal trend with  $\text{PM}_{2.5}$  concentration. Accordingly, the mass ratio of  $\text{NH}_4^+/\text{PM}_{2.5}$  was much higher in the cold season (19%) than in the warm season (8%), similar to that observed in Seoul from the 2012 to 2016.<sup>74</sup> Likewise, in Chinese urban sites,  $\text{NH}_4^+$  and  $\text{PM}_{2.5}$  concentrations were

**Table 2.** Measured and Estimated NH<sub>3</sub> and NH<sub>4</sub><sup>+</sup> Parameters

parameter	warm season	cold season
NH <sub>4</sub> <sup>+</sup> (μg m <sup>-3</sup> )	1.8 ± 0.8	11.7 ± 8.4
f <sub>NH4+</sub>	0	0.5 ± 0.1
δ <sup>15</sup> N (NH <sub>4</sub> <sup>+</sup> ) <sub>measured</sub>	16.4 ± 2.8	4.0 ± 6.1
δ <sup>15</sup> N (NH <sub>3</sub> ) <sub>estimated</sub>	-16.7 ± 3.2	-11.5 ± 3.5

higher in the cold season, but the NH<sub>4</sub><sup>+</sup>/PM<sub>2.5</sub> mass ratio showed less seasonal variation compared to Seoul.<sup>7</sup>

In contrast, δ<sup>15</sup>N (NH<sub>4</sub><sup>+</sup>) values were markedly higher in the warm season than in the cold season with weighted means of 16.4‰ ± 2.8‰ and 4.0‰ ± 6.1‰, respectively, leaving a seasonal difference of 12.4‰. This seasonal pattern of δ<sup>15</sup>N (NH<sub>4</sub><sup>+</sup>) was opposite to that of δ<sup>13</sup>C (Figure 1). Furthermore, δ<sup>15</sup>N (NH<sub>4</sub><sup>+</sup>) was negatively correlated with PM<sub>2.5</sub> changes (Figure 2). This seasonality should be associated with emission sources and/or formation processes that differ seasonally.

The observed seasonal trend in δ<sup>15</sup>N (NH<sub>4</sub><sup>+</sup>) values (Figure 1b) is similar to those reported for Qingyuan Forest (northeast China),<sup>35</sup> urban Beijing (northeast China),<sup>6</sup> Gosan Climate Observatory (an island in South Korea),<sup>75</sup> and urban Wroclaw (Poland),<sup>76</sup> but differs from those reported for urban Guangzhou (China),<sup>77</sup> mountainous Guiyang (China),<sup>78</sup> and rural Alberta (Canada).<sup>43</sup> The annual mean δ<sup>15</sup>N (NH<sub>4</sub><sup>+</sup>) values were below zero in Guangzhou and Guiyang, and relatively low at high temperatures in Alberta. δ<sup>15</sup>N (NH<sub>4</sub><sup>+</sup>) values are thus site-specific and depend mainly on major emission sources and atmospheric NH<sub>3</sub> concentrations.

The seasonal difference in δ<sup>15</sup>N (NH<sub>4</sub><sup>+</sup>) values may be attributed to three factors: (1) the temperature-dependent isotopic-exchange equilibrium factor, ε<sub>NH4+-NH3</sub>; (2) the isotopic fractionation effect, which depends on the NH<sub>3</sub>-NH<sub>4</sub><sup>+</sup> conversion efficiency associated with atmospheric NH<sub>3</sub> levels and chemical composition; and (3) seasonal emission sources.<sup>35,40,44,79</sup>

A phase-equilibrium isotopic-exchange reaction has been suggested as the major pathway for relative <sup>15</sup>N enrichment in NH<sub>4</sub><sup>+</sup> compared to NH<sub>3</sub> in chamber experiments.<sup>79</sup> Consistently, ambient measurements show clearly higher δ<sup>15</sup>N (NH<sub>4</sub><sup>+</sup>) than δ<sup>15</sup>N (NH<sub>3</sub>),<sup>43,44</sup> supporting the phase-equilibrium isotopic-exchange reaction largely responsible for the different δ<sup>15</sup>N values between two phases. If chemical equilibrium is reached with a stoichiometric ratio of NH<sub>3</sub>:H<sub>2</sub>SO<sub>4</sub>, isotopic exchange equilibrium may be attained. The isotopic-exchange equilibrium factor of nitrogen between precursor gas and aerosol (ε<sub>NH4+-NH3</sub>) was theoretically calculated in closed systems as 35‰ at 25 °C;<sup>80</sup> 31‰ ± 4‰ for NH<sub>3(g)</sub> ↔ NH<sub>4(s)</sub><sup>+</sup> and 35‰ ± 4‰ for NH<sub>3(g)</sub> ↔ NH<sub>4(aq)</sub><sup>+</sup> at 20 °C;<sup>81</sup> experimentally determined as +33‰ at 25 °C;<sup>9</sup> and almost equal values were found from field observations<sup>44</sup> and a laboratory experiment using a dynamic chamber.<sup>82</sup> Therefore, a linear fitting relationship between isotopic-exchange equilibrium factor and temperature<sup>40</sup> was employed based on the results of Urey<sup>80</sup> and applied to our seasonal measurements, as follows:

$$\epsilon_{\text{NH4+-NH3}} = (12.4678 \times 1000/T) - 7.6694 \quad (3)$$

where *T* is ambient temperature (Kelvin).

In general, the isotopic fractionation effect increases as temperature decreases. This equation yielded a 3.9‰ higher ε<sub>NH4+-NH3</sub> during the cold season (37.7‰ ± 1.0‰) than

during the warm season (33.8‰ ± 0.5‰), which does not account for the observed seasonal difference of a 12.4‰ higher δ<sup>15</sup>N (NH<sub>4</sub><sup>+</sup>) value in the warm season.

δ<sup>15</sup>N (NH<sub>4</sub><sup>+</sup>) was positively correlated with ambient temperature in the warm season (*R*<sup>2</sup> = 0.40) (SI Figure S4). It seems to indicate volatilization of NH<sub>3</sub> with increasing temperature. In East Asia, NH<sub>3</sub> mixing ratios are generally higher during the warm season,<sup>13,83,84</sup> likely due to emissions from agriculture and urban waste related to NH<sub>3</sub> volatilization by temperature-controlled bacterial enzymatic activity. At high temperatures, NH<sub>3</sub> conversion to NH<sub>4</sub><sup>+</sup> is not favored and particulate NH<sub>4</sub>NO<sub>3</sub> is unstable, leaving more NH<sub>3</sub> than NH<sub>4</sub><sup>+</sup> in the atmosphere.<sup>83</sup> Then, the isotopic equilibrium exchange reaction is more likely to occur, resulting in <sup>15</sup>N enrichment in particle phase. This inference was demonstrated from measurements of δ<sup>15</sup>N for both NH<sub>3</sub> and NH<sub>4</sub><sup>+</sup> at a rural site in Japan, where the annual mean of δ<sup>15</sup>N (NH<sub>4</sub><sup>+</sup>) was 33.3‰ ± 8.2‰ higher than that of δ<sup>15</sup>N (NH<sub>3</sub>) (i.e., Δ<sup>15</sup>N (NH<sub>4</sub><sup>+</sup>-NH<sub>3</sub>) in eq 4) at high NH<sub>3</sub> levels (annual mean NH<sub>3</sub>/NH<sub>4</sub><sup>+</sup> molar ratio of 9.0).<sup>44</sup> On the other hand, in the cold season, the conversion to the particle phase is thermodynamically favorable at low temperature and is further facilitated by the acidity of aqueous-phase aerosol due to abundant acidic gases in the urban atmosphere. Therefore, the δ<sup>15</sup>N (NH<sub>4</sub><sup>+</sup>) and δ<sup>15</sup>N (NH<sub>3</sub>) values of the final mixture can be expressed by an isotopic mass balance for a well-mixed closed system as follows (e.g., Heaton et al.<sup>79</sup> and Pan et al.<sup>18</sup>):

$$\delta^{15}\text{N}(\text{NH}_4^+) = \delta^{15}\text{N}(\text{NH}_3) + \Delta^{15}\text{N}(\text{NH}_4^+ - \text{NH}_3) \quad (4)$$

$$\Delta^{15}\text{N}(\text{NH}_4^+ - \text{NH}_3) = \epsilon_{\text{NH4+-NH3}} \times (1 - f_{\text{NH4+}}) \quad (5)$$

where *f*<sub>NH4+</sub> is the ratio of NH<sub>4</sub><sup>+</sup>/(NH<sub>3</sub> + NH<sub>4</sub><sup>+</sup>) in the atmosphere.

During the warm season, the average *f*<sub>NH4+</sub> was 0.15 ± 0.05 based on ambient NH<sub>3</sub> measurements in Seoul during May–August 2018.<sup>46</sup> Kawashima et al. (2019)<sup>44</sup> reported that the annual-average Δ<sup>15</sup>N (NH<sub>4</sub><sup>+</sup>-NH<sub>3</sub>) is 33.3‰ with *f*<sub>NH4+</sub> < 0.2 and Δ<sup>15</sup>N (NH<sub>4</sub><sup>+</sup>-NH<sub>3</sub>) converges to ε<sub>NH4+-NH3</sub> when *f*<sub>NH4+</sub> is sufficiently small. Therefore, in this study, the δ<sup>15</sup>N (NH<sub>3</sub>) of the warm season was estimated with *f*<sub>NH4+</sub> = 0. The mean *f*<sub>NH4+</sub> for November–December 2020, measured at the NIER site in Seoul, was 0.48<sup>86</sup> and 0.5 ± 0.1 was adopted for the cold-season mean *f*<sub>NH4+</sub>, considering its variability. Finally, the mean δ<sup>15</sup>N (NH<sub>3</sub>) was estimated to be -16.7‰ ± 3.2‰ in the warm season and -11.5‰ ± 3.5‰ (-15.6‰ to -8.1‰) in the cold season (Table 2 and Figure 3).

The *f*<sub>NH4+</sub> value is one of the main causes of uncertainty when estimating contributions of major emission sources of NH<sub>3</sub> from measured δ<sup>15</sup>N (NH<sub>4</sub><sup>+</sup>), unless it was based on simultaneous measurements of NH<sub>3</sub> and NH<sub>4</sub><sup>+</sup> concentrations. The seasonal *f*<sub>NH4+</sub> applied in the present study was similar to reported values in urban Beijing (0.16 in July to 0.64 in January).<sup>84</sup> A slightly increasing pattern of *f*<sub>NH4+</sub> with increasing PM<sub>2.5</sub> concentrations during the warm season (SI Figure S3) was also consistent to warm season *f*<sub>NH4+</sub> variations in urban Beijing (0.1 ± 0.1 for the period of PM<sub>2.5</sub> < 35 μg m<sup>-3</sup> and 0.3 ± 0.05 for 35 μg m<sup>-3</sup> < PM<sub>2.5</sub> < 75 μg m<sup>-3</sup>).<sup>87</sup> These comparable *f*<sub>NH4+</sub> values and seasonal patterns may suggest at some extent a common mechanism governing the NH<sub>3</sub>-NH<sub>4</sub><sup>+</sup> conversion in the urban atmosphere of northeast Asia. In conditions of relatively low atmospheric NH<sub>3</sub> concentrations such as in cold season, gaseous NH<sub>3</sub> may be rapidly absorbed into acidic aqueous-phase aerosols<sup>88</sup> produced from the

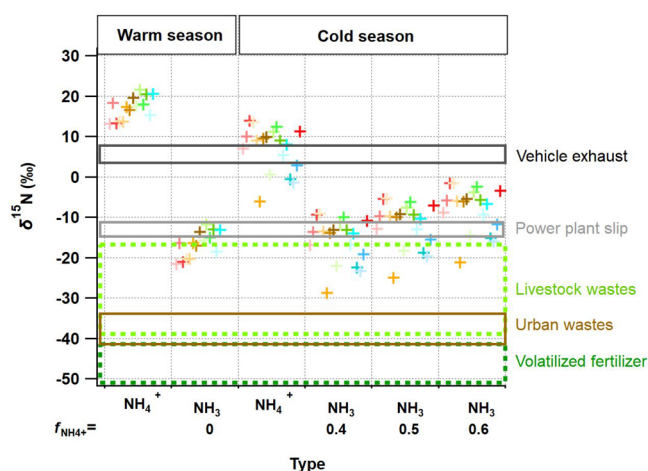


**Figure 3.** Measured  $\delta^{15}\text{N}$  ( $\text{NH}_4^+$ ) values and estimated  $\delta^{15}\text{N}$  ( $\text{NH}_3$ ) values with the most probable  $f_{\text{NH}_4^+}$  value.  $f_{\text{NH}_4^+}$  is seasonally varying with 0 for the warm season and  $0.5 \pm 0.1$  for the cold season (see the text). Different symbol colors indicate different samples. Colored rectangles indicate the  $\delta^{15}\text{N}$  ( $\text{NH}_3$ ) ranges of different source-endmembers ( $6.6\text{‰} \pm 2.1\text{‰}$  for vehicular fossil-related sources,<sup>30</sup>  $-12.95\text{‰} \pm 1.65\text{‰}$  for  $\text{NH}_3$  slip from power-plant equipped with selective catalytic reduction (SCR),<sup>31</sup>  $-46\text{‰} \pm 5\text{‰}$  for volatilized fertilizer,<sup>31,32</sup>  $-28\text{‰} \pm 11\text{‰}$  for livestock waste,<sup>31–33</sup> and  $-37.8\text{‰} \pm 3.6\text{‰}$  for urban waste;<sup>32</sup> SI Table S2).

reactions of increased condensable gases with mineral and/or sea-salt aerosol transported along with northwest winds.<sup>89,90</sup>

Thus,  $\text{NH}_3$  is likely to be consumed before reaching the N isotope equilibrium, leading to  $\delta^{15}\text{N}$  ( $\text{NH}_4^+$ ) values relatively close to the source  $\delta^{15}\text{N}$  ( $\text{NH}_3$ ) values. In contrast, under the abundant atmospheric  $\text{NH}_3$  such as in warm season, the N isotope equilibrium may be achieved, leading to  $^{15}\text{N}$  enrichments in the observed aerosol  $\text{NH}_4^+$ .

In this study, although the warm-season  $\delta^{15}\text{N}$  ( $\text{NH}_3$ ) was slightly lower than the cold-season value, the confidence intervals for the two means were not significantly different. As a result, the seasonal difference of  $12.4\text{‰}$  in  $\delta^{15}\text{N}$  ( $\text{NH}_4^+$ ) observed in Seoul was attributed mainly to isotopic fractionation associated with the conversion of  $\text{NH}_3$  to  $\text{NH}_4^+$ , which implies there is a dominant emission source of  $\text{NH}_3$  throughout the year.

**Emission Sources of Atmospheric  $\text{NH}_3$ .** Based on the  $\delta^{15}\text{N}$  ( $\text{NH}_3$ ) values estimated above, the emission sources of  $\text{NH}_3$  were apportioned using a Bayesian isotopic mixing model with a source-endmember profile (SI Table S2). Recently reported  $\delta^{15}\text{N}$  values of  $\text{NH}_3$  source samples in urban Beijing ( $-37.1\text{‰} \pm 5.0\text{‰}$  for livestock waste,  $-40.4\text{‰} \pm 5.3\text{‰}$  for volatilized fertilizer, and  $-10.6\text{‰} \pm 5.3\text{‰}$  for power-plant  $\text{NH}_3$  slip)<sup>87</sup> were close to the values used in this study.

The simulation results point out that fossil fuel-related emissions are the dominant atmospheric  $\text{NH}_3$  source in Seoul, accounting for  $60\% \pm 26\%$  and  $66\% \pm 22\%$  in the warm season and the cold season, respectively (Figure 4; SI Figure S5). The remaining  $40\% \pm 15\%$  in the warm season and  $34\% \pm 14\%$  in the cold season, is attributed to nonfossil emission sources including volatilized fertilizer, agricultural livestock, and urban waste. Given the seasonal changes in synoptic weather conditions and the variety of  $\text{NH}_3$  sources with a wide range of N isotopic ratios, the insignificant differences in  $\text{NH}_3$  source signatures between the two seasons suggest that fossil fuel-related emissions are the main source of  $\text{NH}_3$  in Seoul. Our

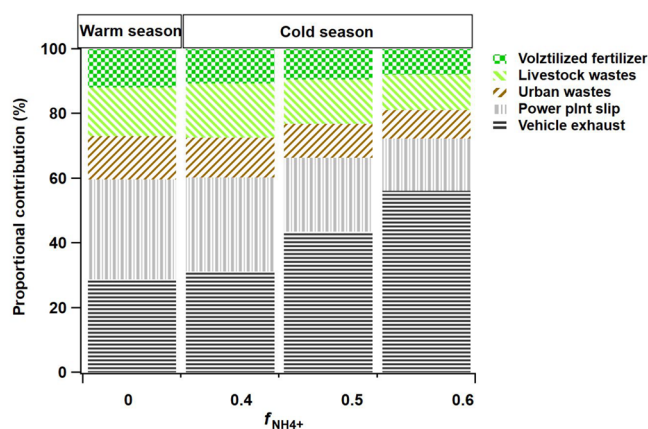


**Figure 4.** Seasonal source apportionment of atmospheric  $\text{NH}_3$  in Seoul, with the most probable  $f_{\text{NH}_4^+}$  value.

source apportionment results are consistent to recent isotope-based studies emphasizing significant contributions (about 50–80%) of urban fossil fuel-related sources to atmospheric  $\text{NH}_3$  in East Asia.<sup>6,12,41,42,87,91</sup> Not to mention, source apportionment based on an isotopic mixing model needs to be treated with caution.<sup>56,92</sup>

The national emission inventory of  $\text{NH}_3$  is yet to be improved, with 63% of  $\text{NH}_3$  being attributed to unidentified area sources other than agricultural sources (15%), vehicular emissions (15%), and combustion sources (7%).<sup>93</sup> Area sources include a broad group of processes such as stationary fuel combustion, cooling towers, material storage, and hospital and laboratory sterilizers that potentially produce emissions from fossil fuels (EPA website; <https://www.epa.gov/air-emissions-inventories/volume-3-area-sources-and-area-source-method-abstracts>). Long-term flux estimates from source regions identified by satellite observations indicate significantly underestimated  $\text{NH}_3$  emissions in current bottom-up inventories, with 67% of identified point sources missing.<sup>94</sup> This isotope-based estimate of the contribution from fossil fuel-related sources is greater than that of the national bottom-up emission inventories of South Korea (22%), but is in line with a recent global  $\text{NH}_3$  emission inventory that highlights that the emission density of  $\text{NH}_3$  is an order of magnitude higher in urban areas than in rural areas.<sup>10</sup> Our finding is in agreement with long-term<sup>12,13,95</sup> or intensive<sup>14</sup> measurement results of atmospheric  $\text{NH}_3$  in China and the U.S. showing large amounts of  $\text{NH}_3$  emissions from urban sources.

$\text{NH}_3$  emissions from vehicle exhaust have been reported in laboratory experiments and on-road measurements as undesirable side effects associated with three-way catalytic converters (TWC) and selective catalytic reduction (SCR) equipped in gasoline powered vehicles and diesel-powered vehicles, respectively.<sup>95–99</sup> The results of the present study are basically in line with a recent study in urban Seoul,<sup>100</sup> where a strong positive correlation ( $R^2 = 0.94$ ) was reported between the  $\text{NH}_3$  concentration and the traffic load multiplied by ambient temperature. The discrepancy between experimental studies and inventories indicates that our current understanding of  $\text{NH}_3$  emissions is poor and further studies are required.

During the warm season, the volatilization of  $\text{NH}_3$  from urban sources is accelerated at higher temperatures and thus, phase-equilibrium isotopic exchange would be promoted by the increased atmospheric  $\text{NH}_3$ , resulting in an enrichment of  $^{15}\text{N}$  in particle-phase  $\text{NH}_4^+$ . Consequently, the estimated  $\delta^{15}\text{N}$

(NH<sub>3</sub>) from the measured  $\delta^{15}\text{N}$  (NH<sub>4</sub><sup>+</sup>) demonstrated the contribution of fossil fuel-related sources to atmospheric NH<sub>3</sub> in Seoul was similar between the warm and cold seasons. During the cold season,  $\delta^{15}\text{N}$  (NH<sub>4</sub><sup>+</sup>) values further decreased with a substantially high contribution of fossil fuels to TC when PM<sub>2.5</sub> was highest (100–140  $\mu\text{g m}^{-3}$ ) (Figure 2). The collective evidence of multiple isotopic analysis highlights common emission sources for NH<sub>3</sub> and carbonaceous compound from fossil fuel-combustion during the highest PM<sub>2.5</sub> pollution periods.

To summarize, this study employed a multiple-isotope approach to quantitatively identify emission sources for NH<sub>4</sub><sup>+</sup> of PM<sub>2.5</sub> in Seoul, one of the megacities in East Asia. The seasonally measured  $\delta^{15}\text{N}$  (NH<sub>4</sub><sup>+</sup>) demonstrates that fossil fuel-related sources including vehicle emissions and power-plant NH<sub>3</sub> slip were dominant, comprising 60%  $\pm$  26% in the warm season and 66%  $\pm$  22% in the cold season. The combined isotopic signatures of  $\delta^{15}\text{N}$  (NH<sub>4</sub><sup>+</sup>) and  $f_{\text{M}}$  and  $\delta^{13}\text{C}$  of TC further suggest vehicle emissions as a main source of NH<sub>4</sub><sup>+</sup>, which was evident during the severe PM<sub>2.5</sub> haze-pollution episodes during the cold season. Therefore, the findings of this study could play a role in bridging the knowledge gap between ambient measurements and bottom-up emission inventories. In recent years, it has been observed that NH<sub>x</sub> concentrations and  $\delta^{15}\text{N}$  (NH<sub>x</sub>) values are vertically varying and subject to regional transport.<sup>42,84,101</sup> Further studies are needed to determine vertical profiles of species-specific isotopic ratios of multiple phases, in conjunction with detailed chemical composition in urban Seoul.

## ■ ASSOCIATED CONTENT

### Supporting Information

The Supporting Information is available free of charge at <https://pubs.acs.org/doi/10.1021/acs.est.1c03903>.

Numbers of measurements of  $f_{\text{M}}$  (TC),  $\delta^{13}\text{C}$  (TC), and  $\delta^{15}\text{N}$  (NH<sub>4</sub><sup>+</sup>); The  $\delta^{15}\text{N}$  values of major NH<sub>3</sub> emission sources; The  $\delta^{13}\text{C}$  values of carbonaceous aerosol emission sources; Monthly variation in meteorological variables, PM<sub>2.5</sub> mass concentration, and isotopic ratios including  $f_{\text{M}}$  (TC),  $\delta^{13}\text{C}$  (TC), and  $\delta^{15}\text{N}$  (NH<sub>4</sub><sup>+</sup>); PSCF results for  $\delta^{13}\text{C}$  (TC) and  $\delta^{15}\text{N}$  (NH<sub>4</sub><sup>+</sup>) with the threshold of the 95th percentile; Box-and-whisker plots of meteorological parameters, gaseous pollutants, TC, TN, TC subfractions, NH<sub>3</sub>, NH<sub>4</sub><sup>+</sup>,  $f_{\text{NH}_4^+}$ , and C and N isotopic composition as a function of PM<sub>2.5</sub> mass concentration; Correlation between  $\delta^{15}\text{N}$  (NH<sub>4</sub><sup>+</sup>) value and ambient temperature for the warm and the cold seasons; Proportional contributions of NH<sub>3</sub> emission sources in the warm and cold season (PDF)

## ■ AUTHOR INFORMATION

### Corresponding Author

Meehye Lee – Department of Earth and Environmental Sciences, Korea University, Seoul 02841, South Korea; [orcid.org/0000-0001-6622-7003](https://orcid.org/0000-0001-6622-7003); Email: [meehye@korea.ac.kr](mailto:meehye@korea.ac.kr)

### Authors

Saehee Lim – Department of Earth and Environmental Sciences, Korea University, Seoul 02841, South Korea  
Joori Hwang – Department of Earth and Environmental Sciences, Korea University, Seoul 02841, South Korea

Claudia I. Czimczik – Department of Earth System Science, University of California, Irvine, Irvine 92697, United States  
Xiaomei Xu – Department of Earth System Science, University of California, Irvine, Irvine 92697, United States  
Joel Savarino – Institute of Environmental Geosciences (IGE), Univ. Grenoble Alpes, CNRS, IRD, Grenoble INP, 38000 Grenoble, France

Complete contact information is available at: <https://pubs.acs.org/10.1021/acs.est.1c03903>

## Notes

The authors declare no competing financial interest.

## ■ ACKNOWLEDGMENTS

This research was supported by the National Strategic Project-Fine Particle of the National Research Foundation of Korea (NRF), funded by the Ministry of Science and ICT (MSIT), Ministry of Environment (ME), and Ministry of Health and Welfare (MOHW) (2017M3D8A1092015). Funding to S.L. was provided by the National Research Foundation of Korea (NRF) from the Ministry of Science and ICT (2018R1D1A1B07050849). M.L. thanks the NRF for the support (2020R1A2C3014592). J.S. acknowledges the partial financial support of the Labex OSUG@2020 (Investissements d'avenir – ANR10 LABX56) and project ANR-15-IDEX-02. Nitrogen isotopic measurements were performed on the PANDA platform (<https://panda.osug.fr/?lang=en>) by Nicolas Caillon and PANDA staff who are acknowledged for their technical support. This is the contribution No. 3 of the PANDA platform. We express our gratitude to Jiye Lee in Eahwa Women's University for making the Lab OC-EC Aerosol Analyzer available for use. We also thank to NIER and KMA for data at their monitoring sites in use.

## ■ REFERENCES

- (1) Kanakidou, M.; Seinfeld, J. H.; Pandis, S. N.; Barnes, I.; Dentener, F. J.; Facchini, M. C.; Van Dingenen, R.; Ervens, B.; Nenes, A.; Nielsen, C. J.; Swietlicki, E.; Putaud, J. P.; Balkanski, Y.; Fuzzi, S.; Horth, J.; Moortgat, G. K.; Winterhalter, R.; Myhre, C. E. L.; Tsigaridis, K.; Vignati, E.; Stephanou, E. G.; Wilson, J. Organic Aerosol and Global Climate Modelling: A Review. *Atmos. Chem. Phys.* **2005**, *5* (4), 1053–1123.
- (2) Jimenez, J. L.; Canagaratna, M. R.; Donahue, N. M.; Prevot, A. S. H.; Zhang, Q.; Kröll, J. H.; DeCarlo, P. F.; Allan, J. D.; Coe, H.; Ng, N. L.; Aiken, A. C.; Docherty, K. S.; Ulbrich, I. M.; Grieshop, A. P.; Robinson, A. L.; Duplissy, J.; Smith, J. D.; Wilson, K. R.; Lanz, V. A.; Hueglin, C.; Sun, Y. L.; Tian, J.; Laaksonen, A.; Raatikainen, T.; Rautiainen, J.; Vaattovaara, P.; Ehn, M.; Kulmala, M.; Tomlinson, J. M.; Collins, D. R.; Cubison, M. J.; Dunlea, J.; Huffman, J. A.; Onasch, T. B.; Alfarra, M. R.; Williams, P. I.; Bower, K.; Kondo, Y.; Schneider, J.; Drewnick, F.; Borrmann, S.; Weimer, S.; Demerjian, K.; Salcedo, D.; Cottrell, L.; Griffin, R.; Takami, A.; Miyoshi, T.; Hatakeyama, S.; Shimono, A.; Sun, J. Y.; Zhang, Y. M.; Dzepina, K.; Kimmel, J. R.; Sueper, D.; Jayne, J. T.; Herndon, S. C.; Trimborn, A. M.; Williams, L. R.; Wood, E. C.; Middlebrook, A. M.; Kolb, C. E.; Baltensperger, U.; Worsnop, D. R. Evolution of Organic Aerosols in the Atmosphere. *Science* (80-). **2009**, *326* (5959), 1525–1529.
- (3) Hallquist, M.; Wenger, J. C.; Baltensperger, U.; Rudich, Y.; Simpson, D.; Claeys, M.; Dommen, J.; Donahue, N. M.; George, C.; Goldstein, A. H.; Hamilton, J. F.; Herrmann, H.; Hoffmann, T.; Iinuma, Y.; Jang, M.; Jenkin, M. E.; Jimenez, J. L.; Kiendler-Scharr, A.; Maenhaut, W.; McFiggans, G.; Mentel, T. F.; Monod, A.; Prévôt, A. S. H.; Seinfeld, J. H.; Surratt, J. D.; Szmigielski, R.; Wildt, J. The Formation, Properties and Impact of Secondary Organic Aerosol:

- Current and Emerging Issues. *Atmos. Chem. Phys.* **2009**, *9* (14), 5155–5236.
- (4) Bond, T. C.; Bhardwaj, E.; Dong, R.; Jogani, R.; Jung, S.; Roden, C.; Streets, D. G.; Trautmann, N. M. Historical Emissions of Black and Organic Carbon Aerosol from Energy-Related Combustion, 1850–2000. *Global Biogeochem. Cycles* **2007**, *21* (2), n/a–n/a.
- (5) Bond, T. C.; Doherty, S. J.; Fahey, D. W.; Forster, P. M.; Bernsten, T.; DeAngelo, B. J.; Flanner, M. G.; Ghan, S.; Kärcher, B.; Koch, D.; Kinne, S.; Kondo, Y.; Quinn, P. K.; Sarofim, M. C.; Schultz, M. G.; Schulz, M.; Venkataraman, C.; Zhang, H.; Zhang, S.; Bellouin, N.; Guttikunda, S. K.; Hopke, P. K.; Jacobson, M. Z.; Kaiser, J. W.; Klimont, Z.; Lohmann, U.; Schwarz, J. P.; Shindell, D.; Storelvmo, T.; Warren, S. G.; Zender, C. S. Bounding the Role of Black Carbon in the Climate System: A Scientific Assessment. *J. Geophys. Res. Atmos.* **2013**, *118* (11), 5380–5552.
- (6) Lim, S.; Yang, X.; Lee, M.; Li, G.; Gao, Y.; Shang, X.; Zhang, K.; Czimeczik, C. I.; Xu, X.; Bae, M.-S.; Moon, K.-J.; Jeon, K. Fossil-Driven Secondary Inorganic PM<sub>2.5</sub> Enhancement in the North China Plain: Evidence from Carbon and Nitrogen Isotopes. *Environ. Pollut.* **2020**, *266*, 115163.
- (7) Liu, Z.; Gao, W.; Yu, Y.; Hu, B.; Xin, J.; Sun, Y.; Wang, L.; Wang, G.; Bi, X.; Zhang, G.; Xu, H.; Cong, Z.; He, J.; Xu, J.; Wang, Y. Characteristics of PM<sub>2.5</sub> Mass Concentrations and Chemical Species in Urban and Background Areas of China: Emerging Results from the CARE-China Network. *Atmos. Chem. Phys.* **2018**, *18* (12), 8849–8871.
- (8) Shao, P.; Tian, H.; Sun, Y.; Liu, H.; Wu, B.; Liu, S.; Liu, X.; Wu, Y.; Liang, W.; Wang, Y.; Gao, J.; Xue, Y.; Bai, X.; Liu, W.; Lin, S.; Hu, G. Characterizing Remarkable Changes of Severe Haze Events and Chemical Compositions in Multi-Size Airborne Particles (PM<sub>11</sub>, PM<sub>2.5</sub> and PM<sub>10</sub>) from January 2013 to 2016–2017 Winter in Beijing, China. *Atmos. Environ.* **2018**, *189*, 133–144.
- (9) Wang, Y.; Wang, Y.; Wang, L.; Petäjä, T.; Zha, Q.; Gong, C.; Li, S.; Pan, Y.; Hu, B.; Xin, J.; Kulmala, M. Increased Inorganic Aerosol Fraction Contributes to Air Pollution and Haze in China. *Atmos. Chem. Phys.* **2019**, *19* (9), 5881–5888.
- (10) Meng, W.; Zhong, Q.; Yun, X.; Zhu, X.; Huang, T.; Shen, H.; Chen, Y.; Chen, H.; Zhou, F.; Liu, J.; Wang, X.; Zeng, E. Y.; Tao, S. Improvement of a Global High-Resolution Ammonia Emission Inventory for Combustion and Industrial Sources with New Data from the Residential and Transportation Sectors. *Environ. Sci. Technol.* **2017**, *51* (5), 2821–2829.
- (11) Zhan, X.; Adalibieke, W.; Cui, X.; Winiwarter, W.; Reis, S.; Zhang, L.; Bai, Z.; Wang, Q.; Huang, W.; Zhou, F. Improved Estimates of Ammonia Emissions from Global Croplands. *Environ. Sci. Technol.* **2021**, *55* (2), 1329–1338.
- (12) Chang, Y.; Zou, Z.; Zhang, Y.; Deng, C.; Hu, J.; Shi, Z.; Dore, A. J.; Collett, J. L. Assessing Contributions of Agricultural and Nonagricultural Emissions to Atmospheric Ammonia in a Chinese Megacity. *Environ. Sci. Technol.* **2019**, *53* (4), 1822–1833.
- (13) Pan, Y.; Tian, S.; Zhao, Y.; Zhang, L.; Zhu, X.; Gao, J.; Huang, W.; Zhou, Y.; Song, Y.; Zhang, Q.; Wang, Y. Identifying Ammonia Hotspots in China Using a National Observation Network. *Environ. Sci. Technol.* **2018**, *52* (7), 3926–3934.
- (14) Sun, K.; Tao, L.; Miller, D. J.; Pan, D.; Golston, L. M.; Zondlo, M. A.; Griffin, R. J.; Wallace, H. W.; Leong, Y. J.; Yang, M. M.; Zhang, Y.; Mauzerall, D. L.; Zhu, T. Vehicle Emissions as an Important Urban Ammonia Source in the United States and China. *Environ. Sci. Technol.* **2017**, *51* (4), 2472–2481.
- (15) Currie, L. A. Evolution and Multidisciplinary Frontiers of <sup>14</sup>C Aerosol Science. *Radiocarbon* **2000**, *42* (1), 115–126.
- (16) Heal, M. R. The Application of Carbon-14 Analyses to the Source Apportionment of Atmospheric Carbonaceous Particulate Matter: A Review. *Anal. Bioanal. Chem.* **2014**, *406* (1), 81–98.
- (17) Mook, W. G.; van der Plicht, J. Reporting <sup>14</sup>C Activities and Concentrations. *Radiocarbon* **1999**, *41* (3), 227–239.
- (18) Pan, Y.; Tian, S.; Liu, D.; Fang, Y.; Zhu, X.; Zhang, Q.; Zheng, B.; Michalski, G.; Wang, Y. Fossil Fuel Combustion-Related Emissions Dominate Atmospheric Ammonia Sources during Severe Haze Episodes: Evidence from <sup>15</sup>N-Stable Isotope in Size-Resolved Aerosol Ammonium. *Environ. Sci. Technol.* **2016**, *50* (15), 8049–8056.
- (19) Widory, D. Combustibles, Fuels and Their Combustion Products: A View through Carbon Isotopes. *Combust. Theory Model.* **2006**, *10* (5), 831–841.
- (20) Chen, Y.-J.; Cai, W.-W.; Huang, G.-P.; Li, J.; Zhang, G. Stable Carbon Isotope of Black Carbon from Typical Emission Sources in China. *Environ. Sci.* **2012**, *33*, 673–678.
- (21) Gleason, J. D.; Kyser, T. K. Stable Isotope Compositions of Gases and Vegetation near Naturally Burning Coal. *Nature* **1984**, *307* (5948), 254–257.
- (22) Tang, G. J. *Characteristics of Carboniferous Coal in North China and Its Palaeogeographic Implications*; Peking, 2001.
- (23) Ahnhotri, R.; Mandal, T. K.; Karapurkar, S. G.; Naja, M.; Gadi, R.; Ahammed, Y. N.; Kumar, A.; Saud, T.; Saxena, M. Stable Carbon and Nitrogen Isotopic Composition of Bulk Aerosols over India and Northern Indian Ocean. *Atmos. Environ.* **2011**, *45* (17), 2828–2835.
- (24) Ancelet, T.; Davy, P. K.; Trompeter, W. J.; Markwitz, A.; Weatherburn, D. C. Carbonaceous Aerosols in an Urban Tunnel. *Atmos. Environ.* **2011**, *45* (26), 4463–4469.
- (25) Ho, K.; Lee, S.; Cao, J.; Li, Y.; Chow, J.; Watson, J.; Fung, K. Variability of Organic and Elemental Carbon, Water Soluble Organic Carbon, and Isotopes in Hong Kong. *Atmos. Chem. Phys.* **2006**, *6* (12), 4569–4576.
- (26) Huang, L.; Brook, J. R.; Zhang, W.; Li, S. M.; Graham, L.; Ernst, D.; Chivulescu, A.; Lu, G. Stable Isotope Measurements of Carbon Fractions (OC/EC) in Airborne Particulate: A New Dimension for Source Characterization and Apportionment. *Atmos. Environ.* **2006**, *40* (15), 2690–2705.
- (27) Kawashima, H.; Haneishi, Y. Effects of Combustion Emissions from the Eurasian Continent in Winter on Seasonal  $\delta^{13}\text{C}$  of Elemental Carbon in Aerosols in Japan. *Atmos. Environ.* **2012**, *46*, 568–579.
- (28) López-Veneroni, D. The Stable Carbon Isotope Composition of PM<sub>2.5</sub> and PM<sub>10</sub> in Mexico City Metropolitan Area Air. *Atmos. Environ.* **2009**, *43* (29), 4491–4502.
- (29) Tanner, R. L.; Miguel, A. H. Carbonaceous Aerosol Sources in Rio de Janeiro. *Aerosol Sci. Technol.* **1989**, *10* (1), 213–223.
- (30) Walters, W. W.; Song, L.; Chai, J.; Fang, Y.; Colombi, N.; Hastings, M. G. Characterizing the Spatiotemporal Nitrogen Stable Isotopic Composition of Ammonia in Vehicle Plumes. *Atmos. Chem. Phys.* **2020**, *20* (19), 11551–11567.
- (31) Felix, D. J.; Elliott, E. M.; Gish, T. J.; McConnell, L. L.; Shaw, S. L. Characterizing the Isotopic Composition of Atmospheric Ammonia Emission Sources Using Passive Samplers and a Combined Oxidation-Bacterial Denitrifier Approach. *Rapid Commun. Mass Spectrom.* **2013**, *27* (20), 2239–2246.
- (32) Chang, Y.; Liu, X.; Deng, C.; Dore, A. J.; Zhuang, G. Source Apportionment of Atmospheric Ammonia before, during, and after the 2014 APEC Summit in Beijing Using Stable Nitrogen Isotope Signatures. *Atmos. Chem. Phys.* **2016**, *16* (18), 11635–11647.
- (33) Freyer, H. D. Preliminary <sup>15</sup>N Studies on Atmospheric Nitrogenous Trace Gases. *Pure Appl. Geophys. PAGEOPH* **1978**, *116* (2–3), 393–404.
- (34) Chen, B.; Andersson, A.; Lee, M.; Kirillova, E. N.; Xiao, Q.; Krusá, M.; Shi, M.; Hu, K.; Lu, Z.; Streets, D. G.; Du, K.; Gustafsson, O. Source Forensics of Black Carbon Aerosols from China. *Environ. Sci. Technol.* **2013**, *47* (16), 9102–9108.
- (35) Huang, S.; Elliott, E. M.; Felix, J. D.; Pan, Y.; Liu, D.; Li, S.; Li, Z.; Zhu, F.; Zhang, N.; Fu, P.; Fang, Y. Seasonal Pattern of Ammonium <sup>15</sup>N Natural Abundance in Precipitation at a Rural Forested Site and Implications for NH<sub>3</sub> Source Partitioning. *Environ. Pollut.* **2019**, *247*, 541–549.
- (36) Jung, J.; Kawamura, K. Springtime Carbon Emission Episodes at the Gosan Background Site Revealed by Total Carbon, Stable Carbon Isotopic Composition, and Thermal Characteristics of Carbonaceous Particles. *Atmos. Chem. Phys.* **2011**, *11* (21), 10911–10928.

- (37) Kirillova, E. N.; Andersson, A.; Han, J.; Lee, M.; Gustafsson, Ö. Sources and Light Absorption of Water-Soluble Organic Carbon Aerosols in the Outflow from Northern China. *Atmos. Chem. Phys.* **2014**, *14* (3), 1413–1422.
- (38) Kundu, S.; Kawamura, K. Seasonal Variations of Stable Carbon Isotopic Composition of Bulk Aerosol Carbon from Gosan Site, Jeju Island in the East China Sea. *Atmos. Environ.* **2014**, *94*, 316–322.
- (39) Lim, S.; Lee, M.; Czimeczik, C. I.; Joo, T.; Holden, S.; Mouteva, G.; Santos, G. M.; Xu, X.; Walker, J.; Kim, S.; Kim, H. S.; Kim, S.; Lee, S. Source Signatures from Combined Isotopic Analyses of PM<sub>2.5</sub> Carbonaceous and Nitrogen Aerosols at the Peri-Urban Taehwa Research Forest, South Korea in Summer and Fall. *Sci. Total Environ.* **2019**, *655*, 1505–1514.
- (40) Pan, Y.; Tian, S.; Liu, D.; Fang, Y.; Zhu, X.; Gao, M.; Gao, J.; Michalski, G.; Wang, Y. Isotopic Evidence for Enhanced Fossil Fuel Sources of Aerosol Ammonium in the Urban Atmosphere. *Environ. Pollut.* **2018**, *238*, 942–947.
- (41) Pan, Y.; Gu, M.; He, Y.; Wu, D.; Liu, C.; Song, L.; Tian, S.; Lü, X.; Sun, Y.; Song, T.; Walters, W. W.; Liu, X.; Martin, N. A.; Zhang, Q.; Fang, Y.; Ferracci, V.; Wang, Y. Revisiting the Concentration Observations and Source Apportionment of Atmospheric Ammonia. *Adv. Atmos. Sci.* **2020**, *37* (9), 933–938.
- (42) Zhang, Y.; Benedict, K. B.; Tang, A.; Sun, Y.; Fang, Y.; Liu, X. Persistent Nonagricultural and Periodic Agricultural Emissions Dominate Sources of Ammonia in Urban Beijing: Evidence from <sup>15</sup>N Stable Isotope in Vertical Profiles. *Environ. Sci. Technol.* **2020**, *54*, 102.
- (43) Savard, M. M.; Cole, A.; Smirnov, A.; Vet, R.  $\delta^{15}\text{N}$  Values of Atmospheric N Species Simultaneously Collected Using Sector-Based Samplers Distant from Sources - Isotopic Inheritance and Fractionation. *Atmos. Environ.* **2017**, *162*, 11–22.
- (44) Kawashima, H. Seasonal Trends of the Stable Nitrogen Isotope Ratio in Particulate Nitrogen Compounds and Their Gaseous Precursors in Akita, Japan. *Tellus B Chem. Phys. Meteorol.* **2019**, *71* (1), 1627846.
- (45) Bhattarai, N.; Wang, S.; Pan, Y.; Xu, Q.; Zhang, Y.; Chang, Y.; Fang, Y.  $\delta^{15}\text{N}$ -Stable Isotope Analysis of NH<sub>x</sub>: An Overview on Analytical Measurements, Source Sampling and Its Source Apportionment. *Front. Environ. Sci. Eng.* **2021**, *15* (6), 1–11.
- (46) NIER. *Improvement of Air Quality Forecast Based on the Measurement -Focused on Secondary Formation of Nitrate NIER-SP2019-088*; Incheon, 2019.
- (47) Xu, X.; Trumbore, S. E.; Zheng, S.; Southon, J. R.; McDuffee, K. E.; Luttgen, M.; Liu, J. C. Modifying a Sealed Tube Zinc Reduction Method for Preparation of AMS Graphite Targets: Reducing Background and Attaining High Precision. *Nucl. Instruments Methods Phys. Res. Sect. B Beam Interact. with Mater. Atoms* **2007**, *259* (1), 320–329.
- (48) Beverly, R. K.; Beaumont, W.; Tausz, D.; Ormsby, K. M.; von Reden, K. F.; Santos, G. M.; Southon, J. R. The Keck Carbon Cycle AMS Laboratory, University of California, Irvine: Status Report. *Radiocarbon* **2010**, *52* (02), 301–309.
- (49) Stuiver, M.; Polach, H. A. Discussion Reporting of <sup>14</sup>C Data. *Radiocarbon* **1977**, *19* (3), 355–363.
- (50) Kaiser, J.; Hastings, M. G.; Houlton, B. Z.; Röckmann, T.; Sigman, D. M. Triple Oxygen Isotope Analysis of Nitrate Using the Denitrifier Method and Thermal Decomposition of N<sub>2</sub>O. *Anal. Chem.* **2007**, *79* (2), 599–607.
- (51) Morin, S.; Savarino, J.; Frey, M. M.; Domine, F.; Jacobi, H.-W.; Kaleschke, L.; Martins, J. M. F. Comprehensive Isotopic Composition of Atmospheric Nitrate in the Atlantic Ocean Boundary Layer from 65°S to 79°N. *J. Geophys. Res.* **2009**, *114* (D5), D05303.
- (52) Zhang, L.; Altabet, M. A.; Wu, T.; Hadas, O. Sensitive Measurement of NH<sub>4</sub><sup>+</sup> <sup>15</sup>N/ <sup>14</sup>N ( $\delta^{15}\text{NH}_4^+$ ) at Natural Abundance Levels in Fresh and Saltwaters. *Anal. Chem.* **2007**, *79* (14), 5297–5303.
- (53) McIlvin, M. R.; Altabet, M. A. Chemical Conversion of Nitrate and Nitrite to Nitrous Oxide for Nitrogen and Oxygen Isotopic Analysis in Freshwater and Seawater. *Anal. Chem.* **2005**, *77* (17), 5589–5595.
- (54) Werner, R. A.; Brand, W. A. Referencing Strategies and Techniques in Stable Isotope Ratio Analysis. *Rapid Commun. Mass Spectrom.* **2001**, *15* (7), 501–519.
- (55) Parnell, A. C.; Phillips, D. L.; Bearhop, S.; Semmens, B. X.; Ward, E. J.; Moore, J. W.; Jackson, A. L.; Grey, J.; Kelly, D. J.; Inger, R. Bayesian Stable Isotope Mixing Models. *Environmetrics* **2013**, *24* (6), 387–399.
- (56) Parnell, A. C.; Inger, R.; Bearhop, S.; Jackson, A. L. Source Partitioning Using Stable Isotopes: Coping with Too Much Variation. *PLoS One* **2010**, *5* (3), No. e9672.
- (57) Stein, A. F.; Draxler, R. R.; Rolph, G. D.; Stunder, B. J. B.; Cohen, M. D.; Ngan, F. NOAA's HYSPLIT Atmospheric Transport and Dispersion Modeling System. *Bull. Am. Meteorol. Soc.* **2015**, *96* (12), 2059–2077.
- (58) Carslaw, D. C.; Ropkins, K. Openair — An R Package for Air Quality Data Analysis. *Environ. Model. Softw.* **2012**, *27–28*, 52–61.
- (59) Kim, S.-W.; Yoon, S.-C.; Kim, J.; Kim, S.-Y. Seasonal and Monthly Variations of Columnar Aerosol Optical Properties over East Asia Determined from Multi-Year MODIS, LIDAR, and AERONET Sun/Sky Radiometer Measurements. *Atmos. Environ.* **2007**, *41* (8), 1634–1651.
- (60) Song, I. H.; Park, J. S.; Park, S. M.; Kim, D. G.; Kim, Y. W.; Shin, H. J. Seasonal Characteristics of PM<sub>1</sub> in Seoul, Korea, Measured Using HR-ToF-Aerosol Mass Spectrometer in 2018. *Atmos. Environ.* **2021**, *266*, 118717.
- (61) Lim, S.; Lee, M.; Savarino, J.; Laj, P. Oxidation Pathways and Emission Sources of Atmospheric Particulate Nitrate in Seoul: Based on  $\delta^{15}\text{N}$  and  $\Delta^{17}\text{O}$  of PM<sub>2.5</sub>. *Atmos. Chem. Phys.* **2022**, in press.
- (62) Zhang, Y.; Ren, H.; Sun, Y.; Cao, F.; Chang, Y.; Liu, S.; Lee, X.; Agrios, K.; Kawamura, K.; Liu, D.; Ren, L.; Du, W.; Wang, Z.; Prévôt, A. S. H.; Szidat, S.; Fu, P. High Contribution of Nonfossil Sources to Submicrometer Organic Aerosols in Beijing, China. *Environ. Sci. Technol.* **2017**, *51* (14), 7842–7852.
- (63) Liu, J.; Li, J.; Zhang, Y.; Liu, D.; Ding, P.; Shen, C.; Shen, K.; He, Q.; Ding, X.; Wang, X.; Chen, D.; Szidat, S.; Zhang, G. Source Apportionment Using Radiocarbon and Organic Tracers for PM<sub>2.5</sub> Carbonaceous Aerosols in Guangzhou, South China: Contrasting Local- and Regional-Scale Haze Events. *Environ. Sci. Technol.* **2014**, *48* (20), 12002–12011.
- (64) Zhang, Y.-L.; Li, J.; Zhang, G.; Zotter, P.; Huang, R.-J.; Tang, J.-H.; Wacker, L.; Prévôt, A. S. H.; Szidat, S. Radiocarbon-Based Source Apportionment of Carbonaceous Aerosols at a Regional Background Site on Hainan Island, South China. *Environ. Sci. Technol.* **2014**, *48* (5), 2651–2659.
- (65) Fisseha, R.; Spahn, H.; Wegener, R.; Hohaus, T.; Brasse, G.; Wissel, H.; Tillmann, R.; Wahner, A.; Koppmann, R.; Kiendler-Scharr, A. Stable Carbon Isotope Composition of Secondary Organic Aerosol from  $\beta$ -Pinene Oxidation. *J. Geophys. Res.* **2009**, *114* (D2), D02304.
- (66) Irei, S.; Huang, L.; Collin, F.; Zhang, W.; Hastie, D.; Rudolph, J. Flow Reactor Studies of the Stable Carbon Isotope Composition of Secondary Particulate Organic Matter Generated by OH-Radical-Induced Reactions of Toluene. *Atmos. Environ.* **2006**, *40* (30), 5858–5867.
- (67) Ancelet, T.; Davy, P. K.; Trompeter, W. J.; Markwitz, A.; Weatherburn, D. C. Carbonaceous Aerosols in a Wood Burning Community in Rural New Zealand. *Atmos. Pollut. Res.* **2013**, *4* (3), 245–249.
- (68) Bird, M. I.; Ascough, P. L. Isotopes in Pyrogenic Carbon: A Review. *Org. Geochem.* **2012**, *42* (12), 1529–1539.
- (69) Das, O.; Wang, Y.; Hsieh, Y. P. Chemical and Carbon Isotopic Characteristics of Ash and Smoke Derived from Burning of C3 and C4 Grasses. *Org. Geochem.* **2010**, *41* (3), 263–269.
- (70) Miyazaki, Y.; Kawamura, K.; Jung, J.; Furutani, H.; Uematsu, M. Latitudinal Distributions of Organic Nitrogen and Organic Carbon in Marine Aerosols over the Western North Pacific. *Atmos. Chem. Phys.* **2011**, *11* (7), 3037–3049.

- (71) Boutton, T. W.; Archer, S. R.; Midwood, A. J.; Zitzer, S. F.; Bol, R.  $\delta^{13}\text{C}$  Values of Soil Organic Carbon and Their Use in Documenting Vegetation Change in a Subtropical Savanna Ecosystem. *Geoderma* **1998**, *82* (1–3), 5–41.
- (72) Aggarwal, S. G.; Kawamura, K. Molecular Distributions and Stable Carbon Isotopic Compositions of Dicarboxylic Acids and Related Compounds in Aerosols from Sapporo, Japan: Implications for Photochemical Aging during Long-Range Atmospheric Transport. *J. Geophys. Res.* **2008**, *113* (D14), D14301.
- (73) Iannone, R.; Koppmann, R.; Rudolph, J. Stable Carbon Kinetic Isotope Effects for the Production of Methacrolein and Methyl Vinyl Ketone from the Gas-Phase Reactions of Isoprene with Ozone and Hydroxyl Radicals. *Atmos. Environ.* **2010**, *44* (34), 4135–4141.
- (74) Bae, C.; Kim, B. U.; Kim, H. C.; Yoo, C.; Kim, S. Long-Range Transport Influence on Key Chemical Components of PM<sub>2.5</sub> in the Seoul Metropolitan Area, South Korea, during the Years 2012–2016. *Atmos. Environ.* **2020**, *Vol. 11*, Page 48 **2020**, *11* (1), 48.
- (75) Kundu, S.; Kawamura, K.; Lee, M. Seasonal Variation of the Concentrations of Nitrogenous Species and Their Nitrogen Isotopic Ratios in Aerosols at Gosan, Jeju Island: Implications for Atmospheric Processing and Source Changes of Aerosols. *J. Geophys. Res.* **2010**, *115* (D20), D20305.
- (76) Cieżka, M.; Modelska, M.; Górka, M.; Trojanowska-Olichwer, A.; Widory, D. Chemical and Isotopic Interpretation of Major Ion Compositions from Precipitation: A One-Year Temporal Monitoring Study in Wrocław, SW Poland. *J. Atmos. Chem.* **2016**, *73* (1), 61–80.
- (77) Jia, G.; Chen, F. Monthly Variations in Nitrogen Isotopes of Ammonium and Nitrate in Wet Deposition at Guangzhou, South China. *Atmos. Environ.* **2010**, *44* (19), 2309–2315.
- (78) Xiao, H.-W.; Xiao, H.-Y.; Long, A.; Wang, Y.-L. Who Controls the Monthly Variations of  $\text{NH}_4^+$  Nitrogen Isotope Composition in Precipitation? *Atmos. Environ.* **2012**, *54*, 201–206.
- (79) Heaton, T. H. E.; Spiro, B.; Robertson, S. M. C. Potential Canopy Influences on the Isotopic Composition of Nitrogen and Sulphur in Atmospheric Deposition. *Oecologia* **1997**, *109* (4), 600–607.
- (80) Urey, H. C. The Thermodynamic Properties of Isotopic Substances. *J. Chem. Soc.* **1947**, *0*, 562.
- (81) Walters, W. W.; Chai, J.; Hastings, M. G. Theoretical Phase Resolved Ammonia-Ammonium Nitrogen Equilibrium Isotope Exchange Fractionations: Applications for Tracking Atmospheric Ammonia Gas-to-Particle Conversion. *ACS Earth Sp. Chem.* **2019**, *3* (1), 79–89.
- (82) Kawashima, H.; Ono, S. Nitrogen Isotope Fractionation from Ammonia Gas to Ammonium in Particulate Ammonium Chloride. *Environ. Sci. Technol.* **2019**, *53* (18), 10629–10635.
- (83) Phan, N.-T.; Kim, K.-H.; Shon, Z.-H.; Jeon, E.-C.; Jung, K.; Kim, N.-J. Analysis of Ammonia Variation in the Urban Atmosphere. *Atmos. Environ.* **2013**, *65*, 177–185.
- (84) Zhang, Y.; Tang, A.; Wang, D.; Wang, Q.; Benedict, K.; Zhang, L.; Liu, D.; Li, Y.; Collett, J. L.; Sun, Y.; Liu, X. The Vertical Variability of Ammonia in Urban Beijing, China. *Atmos. Chem. Phys.* **2018**, *18* (22), 16385–16398.
- (85) Seinfeld, J. H.; Pandis, S. N. *Atmospheric Chemistry and Physics: From Air Pollution to Climate Change*; John Wiley & Sons: New York, 2006.
- (86) NIER. *Formation Mechanisms of Secondary Inorganic Species in Seoul and Gwangju* (20200402006); Incheon, 2021.
- (87) Bhattarai, N.; Wang, S.; Xu, Q.; Dong, Z.; Chang, X.; Jiang, Y.; Zheng, H. Sources of Gaseous  $\text{NH}_3$  in Urban Beijing from Parallel Sampling of  $\text{NH}_3$  and  $\text{NH}_4^+$ , Their Nitrogen Isotope Measurement and Modeling. *Sci. Total Environ.* **2020**, *747*, 141361.
- (88) Wu, Z.; Wang, Y.; Tan, T.; Zhu, Y.; Li, M.; Shang, D.; Wang, H.; Lu, K.; Guo, S.; Zeng, L.; Zhang, Y. Aerosol Liquid Water Driven by Anthropogenic Inorganic Salts: Implying Its Key Role in Haze Formation over the North China Plain. *Environ. Sci. Technol. Lett.* **2018**, *5* (3), 160–166.
- (89) Kang, E.; Park, I.; Lee, Y. J.; Lee, M. Characterization of Atmospheric Particles in Seoul, Korea Using SEM-EDX. *J. Nanosci. Nanotechnol.* **2012**, *12* (7), 6016–6021.
- (90) Lim, S.; Lee, M.; Lee, G.; Kim, S.; Yoon, S.; Kang, K. Ionic and Carbonaceous Compositions of PM<sub>10</sub>, PM<sub>2.5</sub> and PM<sub>1.0</sub> at Gosan ABC Superstation and Their Ratios as Source Signature. *Atmos. Chem. Phys.* **2012**, *12* (4), 2007–2024.
- (91) Park, Y.; Park, K.; Kim, H.; Yu, S.; Noh, S.; Kim, M.; Kim, J.; Ahn, J.; Lee, M.; Seok, K.; Kim, Y. Characterizing Isotopic Compositions of TC-C,  $\text{NO}_3^-$ -N, and  $\text{NH}_4^+$ -N in PM<sub>2.5</sub> in South Korea: Impact of China's Winter Heating. *Environ. Pollut.* **2018**, *233*, 735–744.
- (92) Phillips, D. L.; Gregg, J. W. Uncertainty in Source Partitioning Using Stable Isotopes. *Oecologia* **2001**, *127* (2), 171–179.
- (93) NIER. *Statistics for Emissions of Atmospheric Pollutants in South Korea for Year 2017*; Incheon, 2017.
- (94) Van Damme, M.; Clarisse, L.; Whitburn, S.; Hadji-Lazaro, J.; Hurtmans, D.; Clerbaux, C.; Coheur, P.-F. Industrial and Agricultural Ammonia Point Sources Exposed. *Nature* **2018**, *564* (7734), 99–103.
- (95) Chang, Y.; Zou, Z.; Deng, C.; Huang, K.; Collett, J. L.; Lin, J.; Zhuang, G. The Importance of Vehicle Emissions as a Source of Atmospheric Ammonia in the Megacity of Shanghai. *Atmos. Chem. Phys.* **2016**, *16* (5), 3577–3594.
- (96) Suarez-Bertoa, R.; Mendoza-Villafuerte, P.; Riccobono, F.; Vojtisek, M.; Pechout, M.; Perujo, A.; Astorga, C. On-Road Measurement of  $\text{NH}_3$  Emissions from Gasoline and Diesel Passenger Cars during Real World Driving Conditions. *Atmos. Environ.* **2017**, *166*, 488–497.
- (97) Suarez-Bertoa, R.; Gioria, R.; Selleri, T.; Lilova, V.; Melas, A.; Onishi, Y.; Franzetti, J.; Forloni, F.; Perujo, A.  $\text{NH}_3$  and  $\text{N}_2\text{O}$  Real World Emissions Measurement from a CNG Heavy Duty Vehicle Using On-Board Measurement Systems. *Appl. Sci.* **2021**, *Vol. 11*, Page 10055 **2021**, *11* (21), 10055.
- (98) Suarez-Bertoa, R.; Zardini, A. A.; Astorga, C. Ammonia Exhaust Emissions from Spark Ignition Vehicles over the New European Driving Cycle. *Atmos. Environ.* **2014**, *97*, 43–53.
- (99) Livingston, C.; Rieger, P.; Winer, A.; Livingston, C.; Rieger, P.; Winer, A. Ammonia Emissions from a Representative In-Use Fleet of Light and Medium-Duty Vehicles in the California South Coast Air Basin. *AtmEn* **2009**, *43* (21), 3326–3333.
- (100) Kim, M.; Lim, Y.; Song, I.; Kim, M.; Song, M.; Oh, S.-H.; Lee, T.; Song, M.; Bae, M.-S. Spatial Analysis of Ammonia from Vehicle Measurement in Seoul. *J. Korean Soc. Atmos. Environ.* **2021**, *37* (4), 637–646.
- (101) Wu, L.; Ren, H.; Wang, P.; Chen, J.; Fang, Y.; Hu, W.; Ren, L.; Deng, J.; Song, Y.; Li, J.; Sun, Y.; Wang, Z.; Liu, C.-Q.; Ying, Q.; Fu, P. Aerosol Ammonium in the Urban Boundary Layer in Beijing: Insights from Nitrogen Isotope Ratios and Simulations in Summer 2015. *Environ. Sci. Technol. Lett.* **2019**, *6* (7), 389–395.